[American Journal of Science, Vol. 309, November, 2009, P. 788–833, DOI 10.2475/09.2009.02]

HYDROTHERMAL MINERALS RECORD CO_2 PARTIAL PRESSURES IN THE REYKJANES GEOTHERMAL SYSTEM, ICELAND

ADAM J. E. FREEDMAN*,†, DENNIS K. BIRD*, STEFÁN ARNÓRSSON**, THRÁINN FRIDRIKSSON***, WILFRED A. ELDERS§, and GUDMUNDUR Ó. FRIDLEIFSSON§§

ABSTRACT. **The Reykjanes Peninsula in southwest Iceland is the landward extension of the Mid-Atlantic Ridge spreading center. At present seawater penetrates the coastal Reykjanes geothermal system at depth, where the highest recorded temperature is ~320°C. It mixes with magmatic volatiles and reacts with the basaltic host rock to form secondary hydrothermal minerals in progressively higher-grade mineral alteration zones with increasing depth. Within the epidote-chlorite and portions of the epidote-actinolite zones of alteration, epidote-prehnite-calcite-quartz-fluid constitutes a quadra-variant assemblage that, under conditions of specified temperature, pressure, and activity of H_2O allows prediction of geothermal fluid P_{CO_2} as a function of the composition of the solid solution minerals epidote or prehnite. This assemblage is typically found at temperatures >250°C and ≤310°C, and potentially provides a mineralogical recorder that constrains fluid CO_2 concentrations based on compositional zoning in hydrothermal epidote. Analysis of epidote crystals separated from drillhole-cuttings from three geothermal wells (RN-9, RN-10, RN-17) display complex chemical zoning, generally with Fe(III)-rich cores and Al-rich rims. The Fe(III)-mol fraction of epidote at depths between 0.5 to 1 km ranges from 0.21 to 0.38, between 1 to 2 km depth the range is 0.17 to 0.48 and between 2 to 3 km it is 0.17 to 0.30. The Fe(III)-mol fraction of prehnite ranges from 0.11 to 0.59 in the upper portions of drillhole RN-17, where the highest Fe(III) content in epidote, 0.36, serves as the upper Fe(III) limit for epidotes coexisting with prehnite in this study. Because most observed prehnite crystals in the drillhole-cuttings are too small for electron microprobe analyses (<20μm), we employed a sigmoidal correlation of available compositional data from active geothermal systems to calculate the Fe(III)-Al composition of prehnite using measured compositions of epidote in the Reykjanes system. In drill cuttings that contain epidote, prehnite, quartz and calcite, using measured epidote compositions between the reference temperatures of 275°C and 310°C, calculated values of P_{CO_2} for the geothermal fluids range from ~0.6 to ~6.2 bars. When only epidote, prehnite and quartz are observed in the drill cuttings, the calculated range of P_{CO_2} is from ~1.3 to ~6.8 bars, which provides the maximum value of P_{CO_2} at which calcite will not be present. The present day P_{CO_2} values of geothermal fluids from the Reykjanes system were derived from analytical data on liquid and vapor samples collected at the surface from wet-steam well discharges using both the WATCH and SOLVEQ speciation programs. The geothermal fluids at reference temperature between 275°C and 310°C have P_{CO_2} concentrations ranging from 1.3 bars to 4.0 bars.**

The calculated P_{CO_2} values based on epidote compositions are in close agreement with present-day fluid P_{CO_2} in the Reykjanes geothermal system. 72 percent of the calculated P_{CO_2} values based on epidote compositions where the assemblage of epidote, prehnite, quartz and calcite are observed in drill cuttings are within the range of measured present-day fluids, while 58 percent of the calculated P_{CO_2} values fall within the range when calcite is not present in the drill cuttings. Therefore, our method for calculating fluid P_{CO_2} is proven quite reliable when all four index minerals are

* Department of Geological and Environmental Sciences, Stanford University, Stanford, California 94305, USA
** Institute of Earth Sciences, University of Iceland, Sturlugata 7, 101 Reykjavík, Iceland
*** ÍSOR, Iceland GeoSurvey, Grensásvegur 9, Reykjavík, IS 108 Iceland
§ Department of Earth Sciences, University of California, Riverside, California 92521, USA
§§ HS Orka hf, Brekkustígur 36, 260 Reykjanesbaer, Iceland
† Corresponding author: Stanford University, 450 Serra Mall, Building 320, Room 118, Stanford, California, 94305, USA; freedman.adam@gmail.com

present. Additionally, if only epidote, prehnite and quartz are observed, our model calculations still serve as a moderately accurate predictive proxy for maximum fluid P_{CO_2} composition in the Reykjanes geothermal system.

Ultimately, these correlations between the measured and calculated P_{CO_2} fluid compositions will in the future provide a method, based on compositional variation and paragenesis of hydrothermal minerals in mafic lithologies, by which to characterize spatial and temporal concentrations of CO_2 in both active and fossil hydrothermal systems and in low-grade metamorphic environments.

The generally observed zoning pattern in epidotes in the Reykjanes geothermal system from Fe(III)-rich cores to Al-rich rims suggests that if the zoning formed while equilibrium was maintained among the epidote-prehnite-calcite-quartz assemblage under near isothermal conditions, there must have been an increase in P_{CO_2} with time. This geochemical signature may then be employed to make large scale inferences concerning the evolution of the Reykjanes geothermal system. Analysis of geothermal fluids collected at the wellhead suggest that the four index minerals that comprise the assemblage are in equilibrium with the fluids, thus enabling the application of the P_{CO_2} predictive method discussed in this study to modern epidote samples. In addition to aiding in understanding the history of reactions that involved natural sequestration of CO_2 derived from magmatic degassing, this study may also provide useful insights into reactions that could result from the injection of industrial CO_2-rich fluids into hydrothermal environments in basaltic rocks.

INTRODUCTION

Mid-ocean ridge spreading centers represent a significant natural source of CO_2 from the Earth's mantle due to degassing from upwelling magma. The global mid-ocean ridge CO_2 flux is estimated to be between 1 and $3 \cdot 10^{12}$ mols/year (Marty and Tolstikhin, 1998; Sleep and Zahnle, 2001). Iceland is one of the few places on Earth where this magmatic-hydrothermal environment occurs above sea level (fig. 1). Upwelling magma related to the spreading center and the Iceland Mantle Plume at the exposed ridge is responsible for the formation of Iceland at the center of the North Atlantic Igneous Province (fig. 1; Arnórsson, 1995; White and Morton, 1995; Conrad and others, 2004). Presently the rift zones in Iceland (fig. 1) are characterized by volcanic, seismic and geothermal activity (Pálmason and others, 1985). There are more than twenty high-temperature geothermal systems (>200°C at <1 km depth), including the Reykjanes system in southwest Iceland (fig. 2A; Arnórsson, 1995). Fluid and mineral samples recovered from deep drill holes at the Reykjanes geothermal system permit investigation of mineralogic phase relations that are potential indicators of the concentration of CO_2 released from the magmatic heat source to fluids in the geothermal system.

Extensive investigations and drillings have been conducted at Reykjanes during the last few years for a 100 MWe power plant that was commissioned in May 2006. These drillings provide new opportunities to explore fluid-rock interaction in the deeper parts of this seawater-dominated geothermal system where temperatures exceed 300°C below depths of ~1.5 km (fig. 2B; Franzson and others, 2002; Fridleifsson and Elders, 2005; Hjartarson and Júlíusson, 2007). The geothermal system occurs mainly within basaltic rocks including hyaloclastites, breccias, tuffaceous sediments, lava flows, and pillow lavas (Tómasson and Kristmannsdóttir, 1972). The present day geothermal fluid input is comprised of seawater that has been modified by the addition of magmatic gases and reaction with the host basalts, as well as boiling in the upflow zone (above ~1200 m depth at present); the water-rock interaction has resulted in the formation of a series of mineral alteration zones that increase in grade with depth (see review in Arnórsson, 1995; Bird and Spieler, 2004). These alteration zones are defined by the predominance of a single or several specific secondary minerals as illustrated in figure 3 (Franzson and others, 2002; Fridleifsson and others, 2005).

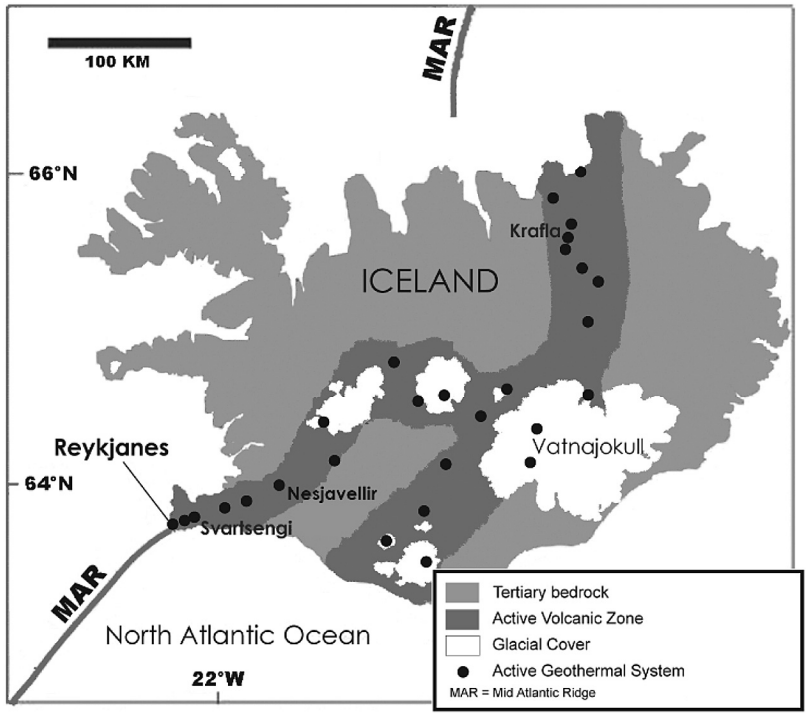

Fig. 1. The distribution of high-temperature geothermal systems within the active volcanic zone of Iceland. The North American and Eurasian plates diverge from one another on either side of the Mid-Atlantic Ridge (MAR). (Adapted from Arnórsson, 1995; Larsen and others, 1998)

Hydrothermal minerals found within the chlorite-epidote and epidote-actinolite alteration zones (see fig. 3) include adularia, albite, anhydrite, calcite, garnet, prehnite, pyrite, and quartz in addition to the minerals characterizing the alteration zones. Calcite is abundant in all wells in the uppermost ~1 km of the system, and occurs sporadically at greater depths. Potentially, several mineral assemblages that include calcite could buffer CO_2 concentrations in the geothermal system (Arnórsson and Gunnlaugsson, 1985; Arnórsson and others, 2007). In this study we focus on a common mineral assemblage found in the Reykjanes geothermal system that consists of Fe(III)-Al epidote, Fe(III)-Al prehnite, calcite and quartz, and the thermodynamic constraints between compositional variations in Ca-Al-Fe(III)-silicates and the CO_2 content of geothermal fluids. For thermodynamic calculations we represent this assemblage by the stoichiometric reaction:

$$\underset{clinozoisite}{Ca_2Al_3Si_3O_{12}(OH)} + \underset{calcite}{CaCO_3} + 1.5\ \underset{quartz}{SiO_2} + H_2O = 1.5\ \underset{prehnite}{Ca_2Al_2Si_3O_{10}(OH)_2} + CO_2 \quad (1)$$

where $Ca_2Al_3Si_3O_{12}(OH)$ represents the component corresponding in composition to clinozoisite in Fe(III)-Al epidote solid solutions, and $Ca_2Al_2Si_3O_{10}(OH)_2$ denotes the Al-end-member component in Fe(III)-Al prehnite solid solutions. At specific temperature, pressure, and activity of liquid water (our chosen standard state for the component H_2O), the equilibrium constant relationship for reaction (1) in the system $NaCl\text{-}CaO\text{-}Al_2O_3\text{-}Fe_2O_3\text{-}SiO_2\text{-}H_2O\text{-}CO_2$ allows prediction of local equilibrium constraints between carbon dioxide (CO_2) concentrations (represented by either aqueous

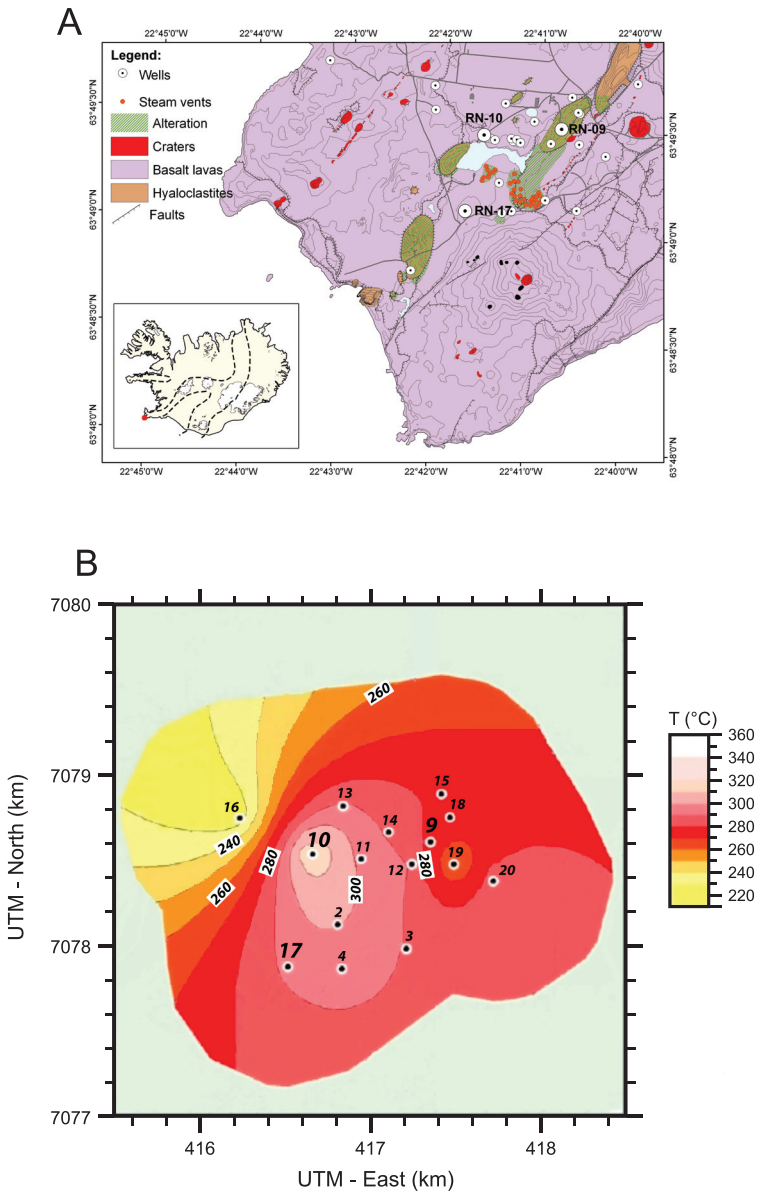

Fig. 2. (A) Generalized geologic map of the Reykjanes Peninsula (map adapted from Karlsdottir, 1998; Saemundsson, 2000; Fridleifsson and others, 2000; and Franzson and others, 2002). Location indicated on inset map by red dot. (B) Map of the Reykjanes drill field showing location of drillholes (by number) and isotherms (°C) at 2200 m depth based on available temperature logs. RN-10 is at the center of the thermal anomaly, RN-17 is to the south and RN-9 to the east. (Adapted from Hjartarson, 2006)

concentrations or the partial pressure of CO_2; we chose the gas standard state for CO_2 in this study, see below) in geothermal fluids and the Fe(III)-Al composition of either epidote or prehnite.

Here we evaluate local equilibrium constraints of reaction (1) on compositional relations among fluid CO_2 and the Fe^{3+}/Al^{3+} content of epidote. Specifically, the

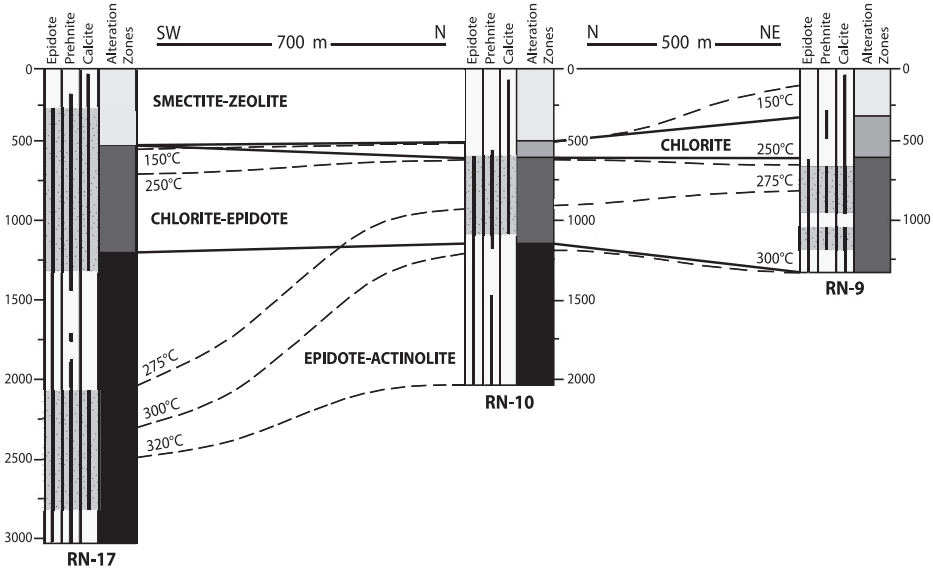

Fig. 3. Cross-section through wells RN-9, RN-10, and RN-17, including mineral alteration zones, distribution of epidote, prehnite and calcite, and isotherms. Distribution of epidote, prehnite and calcite is denoted by the vertical black lines for wells RN-17 (Fridleifsson and others, 2005; Marks, personal communication; Marks and others, 2006), RN-10 (Franzson, 2000; Franzson and others, 2002) and RN-9 (Lonker and others, 1993; Mungania, 1993; Franzson, 2000). The geothermal alteration zones are represented by different shades of gray for each drillhole and are connected by solid lines. Gray stippled bars indicate the depths in wells RN-9, RN-10 and RN-17 where fragments of epidote, prehnite, calcite and quartz have been observed in drill cuttings (see table A1 of the Appendix).

composition of Al and Fe(III) in individual epidote crystals, obtained from drillhole cuttings, allows for predictive calculation of coexisting fluid CO_2 concentration (expressed in this study as partial pressures of CO_2) consistent with equilibrium for reaction (1). This study is based on compositional analysis of epidote crystals from drill cuttings (typical size range ~0.5 to at most 2 mm) from three drillholes (RN-9, RN-10 and RN-17) at the Reykjanes geothermal system. Due to the limited number of analyses conducted on prehnite samples (see below), the compositions of co-existing prehnites employed in the geochemical calculations used to determine fluid CO_2 concentrations consistent with reaction (1) were determined by using compositional correlations observed in other geothermal systems and constraints imposed by the unusually high Fe(III) content of epidote and prehnite in the Reykjanes system. Local equilibrium approximation for the assemblage epidote-prehnite-calcite-quartz is evaluated by comparative analysis between predicted partial pressures of CO_2 (reaction 1) and values constrained by geothermal fluid analyses. Ultimately, local equilibrium constraints of this hydrothermal mineral assemblage can be used to constrain temporal and spatial variations of CO_2 partial pressures in both active and fossil hydrothermal environments.

REYKJANES GEOTHERMAL SYSTEM

Tectonics

Complex local tectonics and volcanism result in significant geothermal activity where the Mid-Atlantic Ridge emerges on land at the Reykjanes peninsula (see figs. 1 and 2A). The volcanic belt that extends along the Reykjanes peninsula is one of the two major active volcanic belts in Iceland. Volcanic activity on the Reykjanes Peninsula is

concentrated on five distinct fissure swarms, but central volcanic complexes associated with evolved magma compositions are notably absent from the four westernmost swarms (Jakobsson and others, 1978). The volcanic fissure swarms of the Reykjanes peninsula run at an angle of about 50° to the direction of plate divergence (Lonker and others, 1993). High-temperature geothermal systems occur in all Reykjanes Peninsula fissure swarms where they intersect the plate boundary. High-level magma chambers have apparently not formed in the Reykjanes volcanic systems (Gudmundsson, 1986, 1987; Arnórsson, 1995), and sheeted dike complexes are likely to serve as the magmatic heat source for the geothermal activity.

Temperature

Temperature distribution at ~2 km depth within the Reykjanes geothermal system is shown in figure 2B. Of the wells specifically considered for the present study, RN-10 is located within the center of the present-day thermal anomaly, while RN-9 is located about 500 m to the east and RN-17 is located approximately 700 m to the south on the flank of the anomaly. Temperatures are in excess of 250°C below ~0.5 km depth in the hottest part of the field, below which the fluids closely follow the seawater boiling point curve for a few hundred meters. At greater depths the fluids remain sub-boiling, increasing in temperature only marginally with depth to the bottom of the drillholes (Hjartarson and Júlíusson, 2007). The measured temperature of RN-9 follows the boiling point curve to about 1000 m, reaching a maximum temperature of 295°C (Mungania, 1993; Franzson, 2000), but remains sub-boiling and at almost constant temperature below that to 1400 m depth at the bottom of the well. In the well RN-10, the temperature follows the boiling point curve from about 500 to 1200 m depth, but remains nearly constant between 310 and 315°C below 1200 m to the bottom of the well at 2054 m (Franzson and others, 2002). The temperature of RN-17 approaches the boiling point curve between 700 and 1100 m depth and then is essentially constant to ~2 km, where the deepest temperature measurements were made, despite the bottom of the well being at 3082 m depth. Because of the plugging and collapse of this well, temperature logging at greater depths was not possible (Fridleifsson and others, 2005). As a consequence, isotherms shown in figure 3 near RN-17 at >2 km are only approximate. The near uniformity of depth to the major mineral zone boundaries between RN-17 and RN-10, as shown in figure 3, suggest that RN-17 is in an area that is experiencing cooling, and that the hydrologic apex of the thermal anomaly has likely migrated northward toward the region near drillhole RN-10.

Fluid Chemistry

The dissolved solids content of the geothermal fluids at Reykjanes is higher than other geothermal waters in Iceland, attributable to seawater recharge (Björnsson and others, 1972; Arnórsson, 1978; Ragnarsdóttir and others, 1984). Concentrations of chloride in the deep geothermal fluid is between ~19,500 and 23,500 ppm (Arnórsson and others, 1978; Arnórsson, 1995; Stefánsson and Arnórsson, 2002). The seawater has undergone chemical modification through interaction with the basaltic host rock (Lonker and others, 1993; Arnórsson, 1995). Boiling in the upflow zone has led to modification of the deep liquid water that essentially includes its degassing and an increase in its dissolved solids content due to steam formation.

Values of δ^2H and $\delta^{18}O$ for geothermal fluids and alteration minerals suggest a more complex history of fluid development. Negative δ^2H values (as low as −23 per mil) have been taken to indicate influx of meteoric fluids throughout the evolution of the system (Ólafsson and Riley, 1978; Sveinbjörnsdóttir, ms 1983a, 1983b; Sveinbjörnsdóttir and others, 1986; Lonker and others, 1993). Fluid inclusion studies on drill cuttings from well RN-9 and RN-10 indicate that dilute fluids dominated the system at

earlier times (Franzson and others, 2002). This, together with analysis of δ^2H of epidote in the systems (Pope and others, 2009) has been interpreted as evidence for meteoric water recharge into the system during the last glaciation. In addition, fluid inclusion data from various minerals at Svartsengi, a geothermal system ~15 kilometers to the east of the Reykjanes system (fig. 1), indicates a significant presence of meteoric water early in the formation of the system and that over time, the salinity of the fluid input has steadily increased (Franzson, 1990).

The pH of unboiled liquid water in the Reykjanes system, as calculated with the aid of the WATCH speciation program (Arnórsson and others, 1982), version 2.1 (Bjarnason, 1994), is usually in the range of 5 to 6, about 1 to 2 pH units below that of meteoric-dominated high-temperature fluids in Iceland [Arnórsson, 1995; see Arnórsson, and others (1982) and Arnórsson and others (2002), for description of the procedure and thermodynamic database employed for calculating the pH]. Computed reservoir pH's reported by Lonker and others (1993) are ~5 (4.88-5.18) at temperatures between 270° and 295°C, consistent with the lower limit cited above. Finally, as we have chosen in this study to represent the chemical potential of CO_2 in the geothermal fluids with the descriptive variable of the partial pressure of CO_2 (P_{CO_2}), we note that reported values computed from combined analysis of vapor and liquid well discharges are between 1.6 to 2.6 bars at reference temperatures of 270 to 295°C (Lonker and others, 1993). Below we report data and computations indicating geothermal reservoir P_{CO_2} values in the range of ~1.3 to 4 bars over the reference temperature range of 275 to 310°C based on analyses from wet-steam well discharges. Carbon dioxide in the geothermal fluids is considered to be largely derived from degassing of upper crustal magmas related to the Iceland mantle plume (Arnórsson, 1995). This has been shown to be the case for dilute meteoric water geothermal systems in Iceland, for example, at Krafla (Ármannson and others, 1982), and comparison of Cl/CO_2 mass ratio in seawater (~240, Krauskopf and Bird, 1995) with that in the Reykjanes geothermal fluid (13.4-28.1; see table 1) indicates that a maximum of 5 to 10 percent of the CO_2 in the Reykjanes system is derived from seawater.

Stratigraphy and Hydrothermal Alteration

The lithostratigraphy of the Reykjanes geothermal system, revealed through drillhole cuttings and logs, consists primarily of basaltic hyaloclastites, breccias, and tuffaceous sediments and basaltic flows, including olivine tholeiitic pillow lavas (Tómasson and Kristmannsdóttir, 1972; Franzson, 2000; Fridleifsson and Albertsson, 2000; Franzson and others, 2002; Fridleifsson and others, 2005). Similar stratigraphic formations are consistently observed across the three Reykjanes geothermal wells RN-9, RN-10, and RN-17 from which epidote and a limited number of prehnite samples were obtained from drill cuttings for the present study.

Reaction of geothermal fluids with the basaltic host rocks has formed a series of progressively higher grade alteration zones with depth, each characterized by distinct mineral assemblages and categorized by the presence of one or more index minerals including smectite, zeolites, chlorite, epidote and actinolite (Kristmannsdóttir, ms, 1970; Lonker and others, 1993; Franzson, 2000; Franzson and others, 2002; Fridleifsson and others, 2005). As illustrated in figure 3 these alteration zones are consistently observed at approximately similar depths in wells RN-9, RN-10 and RN-17 (Lonker and others, 1993; Mungania, 1993; Franzson, 2000; Franzson and others, 2002; Fridleifsson and others, 2005).

It is apparent from the present-day depth distribution of alteration zones and isotherms shown in figure 3 that subsurface temperatures in the region near drillhole RN-17 are lower than peak hydrothermal conditions, possibly reflecting migration of the thermal anomaly northward toward RN-10 (fig. 2B; Franzson and others, 2002; Fridleifsson and others, 2005). Extensive retrograde mineralization is not readily

TABLE 1

Computed deep fluid compositions for selected samples using the SOLVEQ speciation program; corrected for sphalerite and chalcopyrite precipitation during fluid ascent

Well	**RN-19**	**RN-21**	**RN-12**	**RN-23**	**RN-10**
Sample ID	20060386	20060382	20060387	20060371	20030679
Ref T (°C)	275	285	295	300	310
pH	5.408	5.319	5.389	5.277	5.332
Cl^-	5.52E-01	5.35E-01	5.29E-01	5.45E-01	5.30E-01
SO_4^{2-}	2.47E-04	1.86E-04	1.68E-04	1.69E-04	1.11E-04
HCO_3^-	2.02E-02	2.27E-02	3.89E-02	2.55E-02	4.11E-02
HS^-	9.09E-04	1.18E-03	1.66E-03	1.45E-03	2.37E-03
SiO_2 (aq)	9.75E-03	1.11E-02	1.08E-02	1.20E-02	1.24E-02
Al^{3+}	1.76E-06	2.08E-06	1.92E-06	2.98E-06	1.13E-06
Ca^{2+}	4.14E-02	4.00E-02	4.01E-02	4.08E-02	3.84E-02
Mg^{2+}	2.94E-05	2.99E-05	2.73E-05	4.05E-05	5.02E-05
Fe^{2+}	7.96E-06	9.05E-06	8.63E-06	1.30E-05	3.50E-05
K^+	3.67E-02	3.59E-02	3.51E-02	3.68E-02	3.70E-02
Na^+	4.33E-01	4.20E-01	4.13E-01	4.26E-01	4.16E-01
Mn^{2+}	2.21E-05	3.84E-05	3.01E-05	6.03E-05	1.04E-04
Zn^{2+}	6.26E-06	1.26E-05	1.22E-05	3.20E-05	2.89E-05
Cu^+	2.43E-07	6.07E-07	6.17E-07	2.09E-06	7.12E-07
Sr^{2+}	1.04E-04	9.93E-05	1.04E-04	9.86E-05	9.40E-05
Ba^{2+}	5.97E-05	6.56E-05	5.69E-05	7.11E-05	7.97E-05
F^-	9.28E-06	1.01E-05	1.13E-05	1.15E-05	1.25E-05
NH_4^+	7.07E-05	7.48E-05	6.96E-05		1.80E-08
H_3BO_3	7.59E-04	7.42E-04	7.23E-04	8.00E-04	6.92E-04
Activity of H_2O	0.9844	0.9851	0.9856	0.9853	0.986
P_{CO_2} (bar)	1.41	1.5	2.42	1.54	2.34

All concentrations reported in mol/kg of solution.

apparent suggesting that the changing thermal regime is recent. However, the occurrence of prehnite and calcite at depths >2 km in RN-17 in the epidote-actinolite zone are likely due to the recent decrease in temperature. In addition, the localized occurrence of high-temperature minerals including epidote, actinolite and garnet, together with prehnite and calcite, at shallow depths (~350 m) in RN-17 suggest that the uppermost portion of the geothermal system was hotter in the past (Fridleifsson and others, 2005; Marks and others, 2006). The shallow high-temperature alteration is possibly due to elevated hydrostatic pressure caused by an overlying ice sheet in the Pleistocene, which affected the boiling point relationship and allowed for higher temperatures in the shallow subsurface stratigraphy (Fridleifsson and others, 2005; Pope and others, 2009).

The lowest-grade smectite-zeolite alteration zone generally ranges from the surface to a depth of between ~300 and ~500 m. In addition to smectite and a variety of zeolites, this zone contains abundant calcite as shown in figure 4, and quartz is first observed here as well (Franzson, 2000). At depths > 500 m, the Reykjanes system demonstrates progressively higher-grade alteration beginning with the chlorite zone. The chlorite zone extends to ~600 m depth in RN-9 and RN-10, and marks the first appearance of epidote and prehnite, though neither mineral is modally abundant.

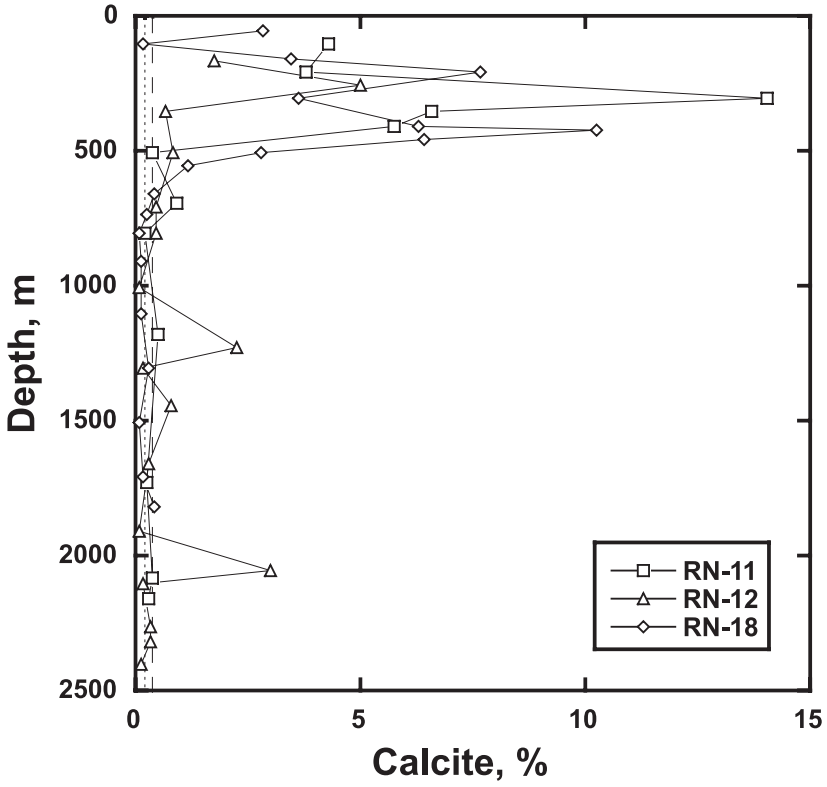

Fig. 4. Modal abundance of calcite in drillhole cuttings for wells RN-11, RN-12 and RN-18 (see fig. 2 for locations) computed based on analysis of total carbon in bulk drill cuttings reported by Wiese and others (2008). Dashed vertical lines represent minimum and maximum background calcite values as determined from bulk rock analyses of basalts in Icelandic outcrops that are not within geothermal systems.

Calcite and quartz occur throughout this zone. A distinct chlorite zone was not observed in the mineralogy of the cuttings from drillhole RN-17 (Fridleifsson and others, 2005). The chlorite-epidote zone ranges from ~600 m to ~1250 m depth. Epidote, prehnite, calcite and quartz are consistently found in this zone (fig. 3), while albite is also present. Below the chlorite-epidote zone is the epidote-actinolite zone, which generally denotes temperatures in excess of ~300°C. Epidote is consistently abundant throughout this zone, while prehnite and calcite are found only intermittently, and garnet first appears here. Below ~2500 m depth, actinolite, epidote, and quartz are the major hydrothermal minerals observed. Brownish colored amphiboles, confirmed as hornblende (Marks and others, 2008) were identified in the lowest part of RN-17 partly replacing pyroxene in diabase intrusions. We note that hematite occurs in at least trace quantities in the drillhole cuttings from the Reykjanes geothermal system (Lonker and others, 1993; Fridleifsson and others, 2005).

Calcite is most abundant in the smectite-zeolite and the chlorite zones, where mineral modes as high as ~14 percent have been computed based on analysis of total C in bulk drill cuttings (see fig. 4; Wiese and others, 2008). Calcite is observed sporadically throughout the chlorite-epidote zone (fig. 3); however, mineral modes are typically less than one percent in this zone; localized zones containing abundant calcite below the chlorite zone do occur, as illustrated in figure 4. In general, calcite is

typically absent, or occurs in trace quantities, in the deeper portions of the epidote-actinolite zone, where temperatures exceed 300°C.

Patches and small veins of albite ($X_{NaAlSi_3O_8}$ = 0.90 to 0.98), oligoclase ($X_{NaAlSi3O8}$ = 0.85 to 0.89), and K-feldspar ($X_{KAlSi_3O_8}$ = 0.91 to 0.98) have been observed in the groundmass host rock, in pore spaces, and replacing primary plagioclase (An_{90}-An_{50}) (Lonker and others, 1993). Albite is the most commonly observed replacement mineral of primary plagioclase in the system (Lonker and others, 1993) and is present throughout each of the alteration zones where temperatures exceed 150°C (Arnórsson, 1995; Fridleifsson and others, 2005).

Mineralogic observations reported above were made on drill hole cuttings that typically range in size from <0.5 to 2 mm at most (and generally decrease in size with increasing drilling depth), thus precluding detailed evaluation of paragenetic sequences of hydrothermal minerals, characterization of coexisting phase relations, and analysis of the time sequence of mineral filled cross cutting fracture systems (veins). Most of the cuttings are of the size of the common and abundant aggregates of epidote crystals. We note that epidote, calcite, and quartz are locally abundant and readily identified, whereas the trace quantities of prehnite in ground mass and vesicles/fractures are at best difficult to identify in the drill cuttings.

In summary, the following depth ranges correspond to approximate depths where epidote, prehnite, calcite, and quartz have all been identified in drill cuttings from the wells shown in figure 2B: RN-9: 700 to 925 m, 1100 to 1200; RN-10: 600 to 1100 m; RN-17: 275 to 1300 m, 2175 to 2825 m (Lonker and others, 1993; Mungania, 1993; Franzson, 2000; Franzson and others, 2002; Fridleifsson and others, 2005). These depth ranges are shown graphically by the gray stippled bars in the cross sections of figure 3.

MINERAL CHEMISTRY OF EPIDOTE AND PREHNITE

Within the Reykjanes geothermal system epidote and prehnite both display compositions with varying degrees of Al and Fe(III) substitution (Sveinbjörnsdottir, 1992; Lonker and others, 1993). Lonker and others (1993) note that epidotes formed in vesicles, veins and as pseudomorphic replacements within the basaltic host rocks are not significantly different in composition. Here we review the mineral chemistry of epidote and prehnite relevant to their paragenesis in the Reykjanes geothermal system.

Epidote has a formula of $Ca_2Fe_xAl_{3-x}Si_3O_{12}(OH)$, where x represents the number of atoms of Fe(III) substituted for Al in the M1 and M3 crystallographic sites. The iron is almost exclusively in the trivalent state as deduced by crystal chemical and spectral analysis (see reviews by Franz and Liebscher, 2004; Liebscher, 2004). Several studies have shown that the Fe(III) atoms are distributed almost exclusively in the largest and most distorted M3 site, and to a lesser extent in the M1 site. Rarely, and only at high temperature does Fe(III) enter the M2 site, which under the vast majority of conditions contains only Al (Dollase, 1973; Bird and others, 1988; Patrier and others, 1991; Fehr and Heuss-Aßhichler, 1997; Giuli and others, 1999; Gottschalk, 2004).

Two common end-members components of epidote solid solutions are *clinozoisite* ($Ca_2Al_3Si_3O_{12}(OH)$) and *epidote* ($Ca_2Al_2FeSi_3O_{12}(OH)$); most natural epidotes are compositionally between these end-members. The composition of Fe-epidote ($Ca_2Fe_3Si_3O_{12}(OH)$), referred to as *pistacite,* does not occur in nature, but is a useful theoretical end-member for natural epidotes more Fe(III)-rich than ($Ca_2Al_2FeSi_3O_{12}(OH)$. The notation of X_{ps} is used here to denote the mole fraction of the *pistacite* component in natural epidotes, where X_{ps} is equal to $n_{Fe}/(n_{Fe} + n_{Al})$ and n_{Fe} and n_{Al} represent the number of atoms of Fe and Al per formula unit respectively.

Epidote commonly forms in active geothermal systems as the product of reactions between hydrothermal solutions and Ca-bearing phases in the host rocks, such as

plagioclase or calcite (Arnason and others, 1993; Bird and Spieler, 2004). In the basalt hosted geothermal systems of Iceland, epidote typically occurs as yellowish green, xenoblastic crystals (<0.8 mm) and as radiating crystal aggregates (25-250 μm) often replacing plagioclase and filling vesicles and veins as a secondary alteration mineral (Tómasson and Kristmannsdóttir, 1972; Ragnarsdóttir and others, 1984; Sveinbjörnsdóttir, 1992; Lonker and others, 1993; Bird and Spieler, 2004). Although complex compositional zoning is observed (for example, see fig. 5), an overwhelming proportion of epidotes formed from altered basalt in active geothermal systems in Iceland, as well as in early Tertiary hydrothermal systems in East Greenland, are zoned with Al-rich rims and Fe(III)-rich cores (see figs. 5 and 6; Hreggvidsdóttir, 1987; Arnason and Bird, 1992; Lonker and others, 1993).

Analyses from previous studies of epidote composition from the seawater dominated Reykjanes system indicate an X_{ps} range of between 0.20 and 0.32, with the exception of two Fe-rich (X_{ps} = 0.37 and 0.47) analyses (Sveinbjörnsdóttir, 1992; Lonker and others, 1993). Previously analyzed epidote samples from the dilute, meteoric fluid dominated Krafla system are similar to those at Reykjanes and have an X_{ps} range of between 0.20 and 0.32 (Sveinbjörnsdóttir, 1992). Therefore, apart from the two especially Fe-rich analyses, results from these prior studies of epidote compositions from the Reykjanes and Krafla systems suggest that the salinity of the geothermal fluids is not a controlling factor on the range of the chemical composition of epidote solid solution in these two systems. We note that previous studies of epidote composition in active geothermal systems (including the data presented in this study) indicates a near complete compositional variation of Fe(III)-Al substitution in epidote solid solutions (for example, Bird and Helgeson, 1980; Bird and others, 1984, 1988; Bird and Spieler, 2004) and that there is no obvious compositional (miscibility) gaps as noted in some low-grade metamorphic environments (see review and summary in Grapes and Hoskin, 2004).

Prehnite has the general stoichiometry of $Ca_2Al_{1-x}Fe_x(AlSi_3O_{10})(OH)_2$ where x denotes moles of Fe(III) substituted for octahedral Al. Other than Fe(III) substitution in the M1 site, which has been reported as high as 60 mole percent (Deer and others, 1962; Hashimoto, 1964; Surdam, 1969), there is little substitution of other elements into the prehnite structure. Prehnite commonly occurs as a secondary mineral in basalt and related rocks (Klein, 2002). Prehnite has been observed in trace quantities in drill cuttings from all the drillholes in the Reykjanes geothermal system (Mungania, 1993; Lonker and others, 1993; Franzson and others, 2002; Fridleifsson and others, 2005). It typically occurs as light green, sheaf-like aggregates in open space fillings and veins that have been found to crosscut albite veins. Compositions reported by Lonker and others (1993) from drillholes RN-8 and RN-9 range from 0.08 to 0.28 moles of Fe(III) per formula unit (which is equivalent to the mole fraction of Fe-prehnite, $X_{Fe,Prehnite} = n_{Fe}$). Marks (personal communication/and others, 2006) report a range of $X_{Fe,Prehnite}$ between 0.15 and 0.55 in the upper portions of drillhole RN-17. Because of the small size of drill cuttings (< ~2 mm) and the small modes of prehnite, the modal distribution and paragenesis of prehnite is difficult to characterize. It has been noted from petrographic analysis of drill cuttings from well RN-9 that both Fe(III)-rich and Fe(III)-poor prehnite occurs in veins that crosscut albite veins; and textural evidence suggests local replacement of prehnite by calcite (Lonker and others, 1993; Mungania, 1993).

COMPOSITION OF EPIDOTE AND PREHNITE

Analytical Procedures

Electron microprobe analysis was used to determine the mineral chemistry of epidote and prehnite, particularly with regard to octahedral substitution of Al and

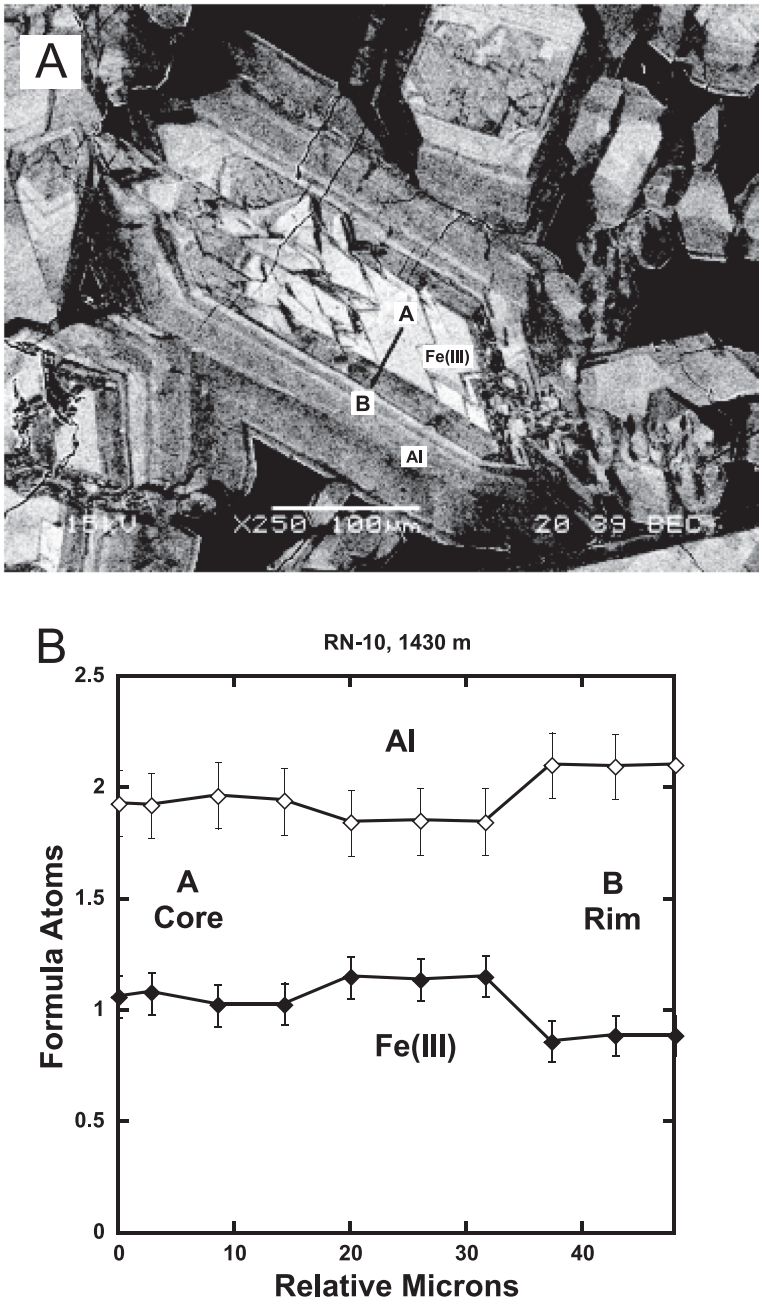

Fig. 5. (A) Back-scattered electron photomicrograph showing complex oscillatory zoned epidote with Fe(III)-rich cores and Al-rich rims from 1430 m depth in well RN-10 at Reykjanes. The solid line marked A—B shows the traverse of the probe scan in which data was gathered approximately every 5.5 microns (see fig. 5B). The darker color around the rim indicates an Al-rich region, while the light colored core indicates an Fe(III)-rich region. (B) Quantitative analysis of microprobe scan reflecting relative amounts of Al (open diamonds) and Fe(III) (filled diamonds) across the crystal shown in figure 5A. The mirror image of Al and Fe(III) demonstrates the substitution by one another in octahedral sites of the epidote crystal. Oxide weight percent errors are 1–2% of the amount measured, and have been extrapolated for formula atoms.

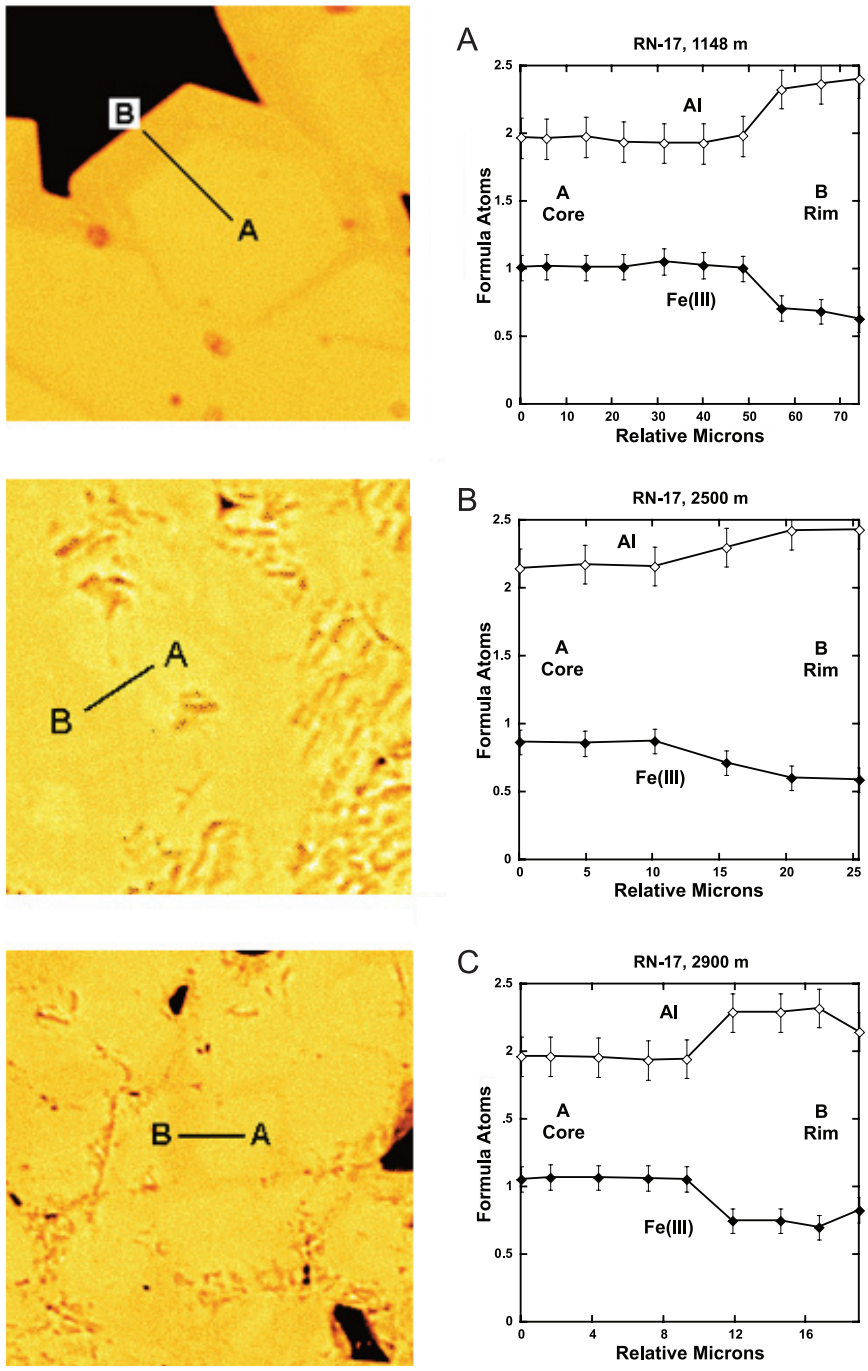

Fig. 6. Electron microprobe scan measurements and quantitative analysis of core to rim zoning in various epidote crystals from RN-17 at depths of (A) 1148 m (B) 2500 m and (C) 2900 m.

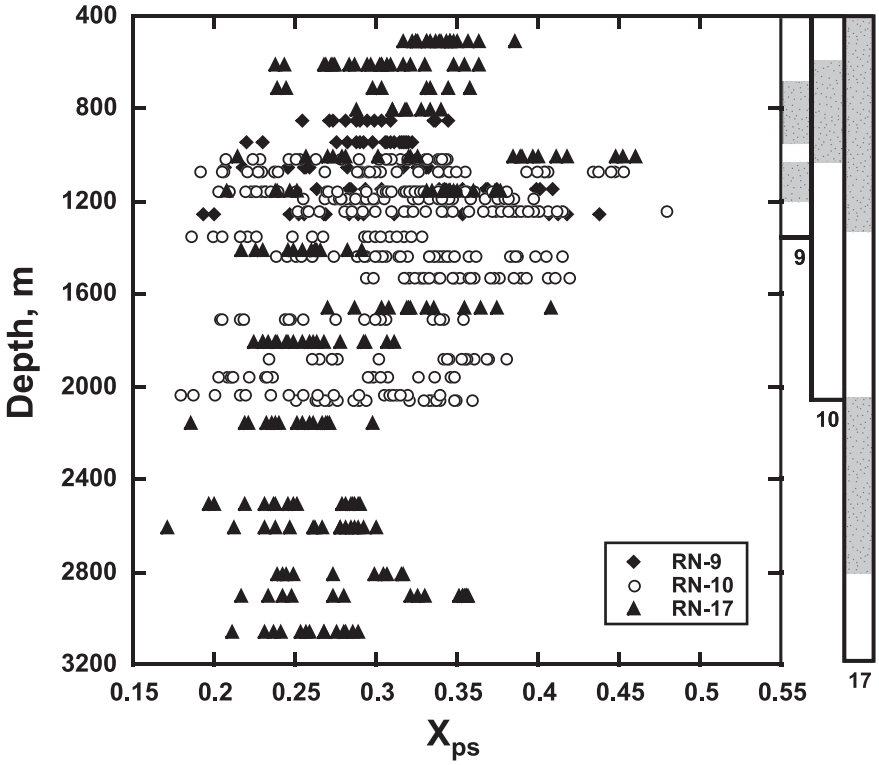

Fig. 7. Compilation of epidote X_{ps} ($n_{Fe}/(n_{Al} + n_{Fe})$) as a function of depth from wells RN-9, RN-10 and RN-17 in the Reykjanes geothermal system. Gray stippled bars to the right indicate the depths in wells RN-9, RN-10 and RN-17 where fragments of epidote, prehnite, calcite and quartz have been observed in drill cuttings (see fig. 3 and table A1 of the Appendix for details).

Fe(III) (figs. 5B and 6). Analyses were conducted on an automated JEOL 733A electron microprobe at Stanford University operated at 15 kV accelerating potential and 15 nA beam current. Calibration was conducted using natural geologic standards from the Stanford Microprobe Collection (Mg, Si, Ca: diopside; Na: albite; K: orthoclase; Al, Mn: spessartine garnet; Fe: magnetite; Ti: rutile; Cr: chromite). Beam diameter for analysis of epidotes and prehnites was 2 to 3 microns. Raw counts were collected for 20 seconds at each point and element distribution was converted to oxide percents and formula atoms based on 12.5 oxygens for epidote and the 11 oxygens for prehnite. The total Al (n_{Al}) and Fe(III) (n_{Fe}) detected in epidote analyses were normalized to three octahedral sites.

Epidote Composition

A summary of the Al and Fe(III) content and the corresponding mole fraction of the Fe(III) end member, X_{ps} ($X_{ps} = n_{Fe}/(n_{Al} + n_{Fe})$), of analyzed epidotes from RN-9, RN-10 and RN-17 drillcuttings are reported in table A1 of the Appendix and shown graphically in figure 7 as a function of depth. Representative epidote analyses are reported in table A2 of the Appendix, including one sample from each of the three RN wells. The general compositional trend characteristic of this geothermal system is for individual epidote crystals to display Fe(III)-rich cores and Al-rich rims (fig. 6), although oscillatory zoning reflecting irregular fluctuations in Al-Fe(III) substitution in epidote crystals has also been observed (fig. 5A).

RN-9 epidotes display strong core-rim zoning with Fe(III)-rich cores and Al-rich rims at all depths, though to a greater extent with depth. The analyzed RN-9 epidotes from above 1 km depth exhibit an X_{ps} range of 0.21 to 0.34, while the X_{ps} values of samples from below 1 km depth extend from 0.19 to 0.44. The RN-10 epidotes from 1 to 2 km depth also have Al-rich rims and Fe(III)-rich cores and compositions range from X_{ps} of 0.18 to 0.48.

In RN-17, above 1 km depth, epidotes are all mostly Fe(III)-rich, ranging in a similar fashion to RN-9 samples from an X_{ps} of 0.24 to 0.38. From 1 to 2 km depth, however, the samples exhibit Fe(III)-rich core and Al-rich rim zoning and the compositions extend over a wider range from X_{ps} of 0.21 to 0.46. These values are very similar to the compositional range observed in both RN-9 and RN-10 at the same depths. Unlike the epidote samples from $<$ 2 km depth, the RN-17 samples from 2 to 3 km depth do not exhibit Al-Fe(III) zoning, nor do they exhibit such high Fe(III) concentration, ranging in X_{ps} from 0.17 to 0.36.

Prehnite Composition

Analyses of Al and Fe(III) content in prehnite samples from RN-17 are reported in table A3 of the Appendix and shown in figure 8 (open squares with diagonal lines) as a function of depth. The prehnite compositions ($X_{Fe,Prehnite} = n_{Fe}$) in RN-17 at depths of 700 and 800 m range from $X_{Fe,Prehnite}$ of 0.13 to 0.59. A similar compositional range of $X_{Fe,Prehnite}$ of 0.15 to 0.55 is reported by Marks and others (personal communication/2006) at a depth of 550 m in RN-17, and Lonker and others (1993) report a compositional range of $X_{Fe,Prehnite}$ between ~0.08 and 0.28 from drillholes RN-8 and RN-9. Due to the scarcity and small grain size (~20 μm) of prehnite crystals in drill cuttings, it was not possible to directly observe whether compositional core-rim zoning patterns are present in prehnite crystals. However, measured prehnite compositions do demonstrate an extreme range of Fe(III)-Al substitution similar to that of epidotes in the Reykjanes geothermal system.

THERMODYNAMIC CONSIDERATIONS

In hydrothermal environments the Fe(III)-Al composition of epidote and prehnite are a sensitive function of temperature, pressure, bulk rock composition, fluid composition (especially redox state, CO_2 concentration, and pH), and metastable phase relations controlled by reaction kinetics (Bird and Helgeson, 1980, 1981; Arnason and others, 1993; Bird and Spieler, 2004; Grapes and Hoskin, 2004). Minor changes in pH have been found to play an influential role in controlling Fe(III)-Al zoning in epidotes in basaltic host rocks, where plagioclase hydrolysis causes a decrease in the pH (as OH^- is consumed to form Al-hydroxide species) and in the activity ratio of aqueous $Fe(OH)_3/Al(OH)_4^-$, leading to zoning with Al-rich rims (Arnason and Bird, 1992). The theoretical analysis employed by Arnason and Bird (1992), however, did not include CO_2 as a component during the irreversible hydrolysis of plagioclase.

The Reykjanes geothermal system represents an open thermodynamic system in which other factors, including variable flux of CO_2 from magmatic sources (diking events), likely play an important role in determining the extent to which compositional zoning in epidote occurs. With this in mind we focus on local equilibrium constraints imposed by reaction (1) on CO_2 in geothermal fluids and epidote composition. Below, we demonstrate that at constant temperature and pressure, an increase in CO_2 of geothermal fluids requires the Al content of epidote and prehnite to increase in order to maintain equilibrium for the assemblage epidote-prehnite-calcite-quartz.

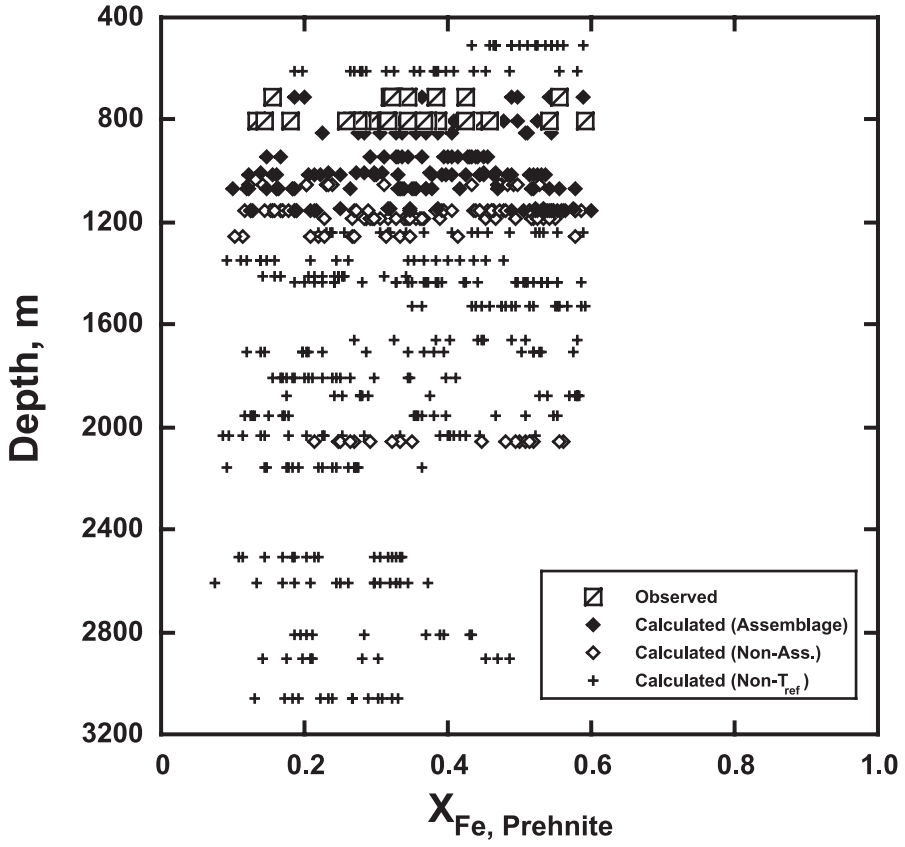

Fig. 8. Calculated (diamonds and crosses) and measured (squares) $X_{Fe,Prehnite}$ values as a function of depth in wells RN-9, RN-10 and RN-17. The measured values are from RN-17, but the calculated values have been derived from epidote compositions in RN-9, RN-10 and RN-17 using equations (16) and (20). The solid diamonds (marked "assemblage") are computed from measured compositions of epidotes at depths where prehnite, quartz and calcite are also found in the drill cuttings, and the open diamonds (marked "non-assemblage") are from depths where prehnite and/or calcite are absent from the cuttings (see figs. 3 and 7). Only samples found in cuttings at depths where reference temperatures range between 275 and 310°C are denoted as "assemblage" or "non-assemblage." All other values are labeled as "Non-T_{Ref}."

Phase Rule Constraints and Thermodynamic Conventions

Equilibrium for the assemblage epidote-prehnite-calcite-quartz-fluid, as represented by reaction (1), is used to evaluate the relationship between fluid CO_2 content and epidote composition. First we consider phase rule constraints:

$$f = c + 2 - p, \tag{2}$$

where f is the variance (independent variables), c is the minimum number of chemical components and p is the number of phases. Equilibrium denoted by reaction (1) for the Reykjanes geothermal system can be represented using 7 components (NaCl, CaO, Al_2O_3, Fe_2O_3, SiO_2, H_2O, and CO_2) to describe the compositions of the 5 phases (calcite, epidote, prehnite, quartz, and fluid) such that equation (2) becomes $f = 7 + 2 - 5 = 4$. The assemblage is quadra-variant; by fixing four intensive variables (for example, temperature, pressure, the activity of H_2O in the fluid phase, and either epidote or prehnite composition), the equilibrium is uniquely defined. In the present

study, observed temperature and pressure profiles in wells are constrained as a function of depth in the drillholes, activity of H_2O is computed using aqueous species distribution algorithms and the composition of the geothermal fluid (see below), and epidote compositions are measured by microprobe analysis of crystals obtained from drillhole cuttings (the composition of prehnite is computed from equations and data given below) to calculate the fugacity of CO_2 in the geothermal fluids in equilibrium with this assemblage (see details below).

The following standard state conventions are adopted: unit activity of pure minerals and liquid H_2O at any temperature and pressure, and for CO_2 unit fugacity of the pure gas at 1 bar and any temperature (see for example, Helgeson and others, 1978). The latter standard state chosen for CO_2 facilitates comparative analysis between values determined from drillhole discharge fluids and mineralogic constraints (reaction 1). We take the activities of $CaCO_3$ and SiO_2 components in calcite and quartz, respectively, to be equal to unity, and for the activity of H_2O in the geothermal fluid we use a value of ~0.985 computed by the aqueous geochemical system modeling program, SOLVEQ (Reed, 1982), for the five fluid samples listed in table 1 and all P_{CO_2} calculations using equation (3). In reaction (1) activities of components corresponding in composition to clinozoisite ($Ca_2Al_3Si_3O_{12}(OH)$) and Al-prehnite ($Ca_2Fe(AlSi_3O_{10})(OH)_2$) in Fe(III)-Al epidote and Fe(III)-Al prehnite solid solutions, respectively, are computed from measured compositions of epidote and prehnite reported in the Appendix (tables A1 and A3) using equations and data presented below. Due to the distribution of trace quantities of hematite in drill cuttings at Reykjanes reported by Lonker and others (1993), Franzson and others (2002), and Fridleifsson and others (2005), we do not consider oxygen fugacity as a descriptive variable governing Fe(III)-Al composition of epidote solid solutions.

The equilibrium constant, K, for reaction (1) adopted in this study is computed using a temperature-dependent algorithm provided by Arnórsson and others (2007): $\text{Log K} = 57.781 - 22843/T^2 - 4792.99/T + 0.00829\,T + 0.6864 \times 10^{-6}\,T^2 - 19.302\,\text{LogT}$. The algorithm was derived using thermodynamic properties of minerals reported by Holland and Powell (1998), for H_2O from the SUPCRT computer program (Johnson and others, 1992), and for $CO_{2,g}$ from Robie and Hemingway (1995), at temperatures corresponding to liquid-vapor equilibrium for H_2O. Assuming ideal gas behavior for CO_2 (computed fugacity coefficients, λ, for CO_2 are 0.975), the equilibrium constant relationship for reaction (1) can be expressed as:

$$\text{Log}(\lambda \cdot P_{CO_2}) = \text{Log}(\lambda) + \text{Log}(P_{CO_2}) = \log f_{CO_2}$$
$$= \log K_{T,P} + \log a_{czo} - \frac{3}{2}\log a_{preh} + \log a_{H_2O}, \quad (3)$$

where P_{CO_2} is the partial pressure of CO_2 and f_{CO_2} the fugacity of CO_2 in the geothermal fluid, λ is the fugacity coefficient, $K_{T,P}$ is the equilibrium constant for reaction (1), a_{czo} is the thermodynamic activity of the clinozoisite component in epidote, a_{preh} is the thermodynamic activity of Al-prehnite in prehnite, and a_{H_2O} is the activity of H_2O referenced to the liquid standard state described above.

Activity-Composition Relations

Epidote.—Determining the thermodynamic activity of the $Ca_2Al_3Si_3O_{12}(OH)$ (clinozoisite) component (a_{czo}) of epidote solid solutions over a compositional range of X_{ps} between 0.17 and 0.48 (fig. 9) is required for calculating P_{CO_2} using equation (3). If one designates completely "ordered" epidote as containing Fe(III) in only the M3 site, then the octahedral "disordering" of epidote that induces crystal lattice distortion with increasing temperature can be represented by:

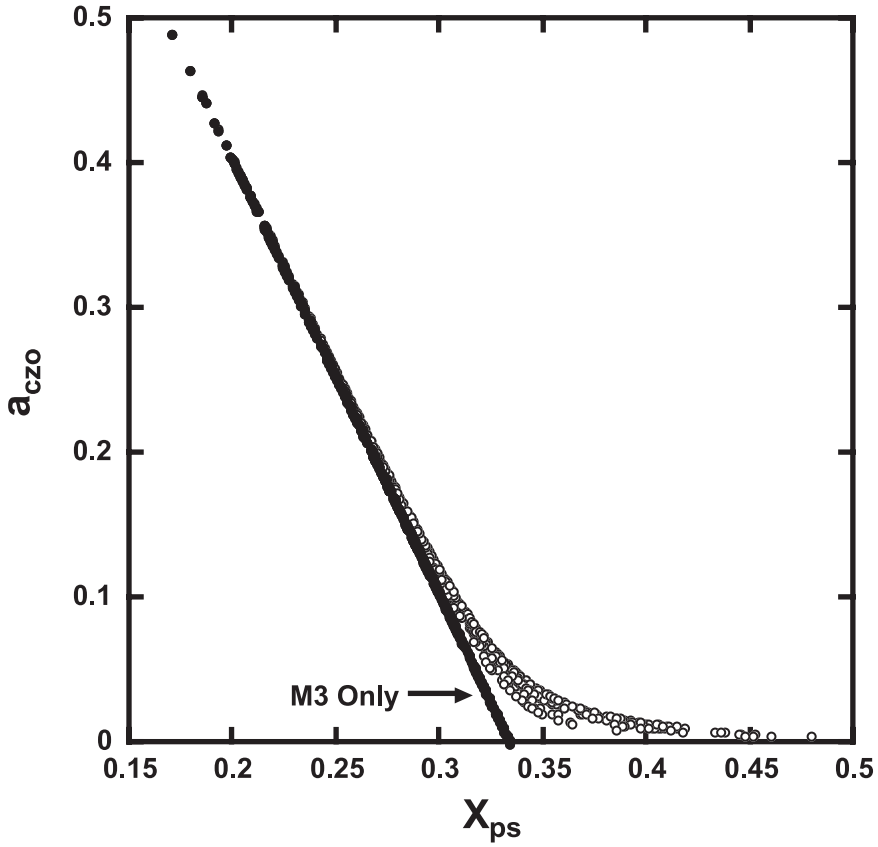

Fig. 9. Calculated activities of the clinozoisite component in epidote solid solutions assuming Fe(III) is restricted to the M3 site (solid circles) and for intracrystalline equilibrium distribution of Fe(III) between the M1 and M3 sites (open circles). The "M3 Only" symbol applies the relationship $a_{czo} = 1\text{–}3 \cdot X_{ps}$, which assumes that Fe(III) exclusively substitutes for Al into the M3 octahedral site. The open circles represent the relationship $a_{czo} = X_{Al,M1} \cdot X_{Al,M3}$, which accounts for the fact that though Fe(III) substitutes largely into the M3 site, it also substitutes into the M1 site on a limited basis. (See text for details).

$$Ca_2Al^{M1}Al^{M2}Fe^{M3}Si_3O_{12}(OH) = Ca_2(Al_{1-x}Fe_x)^{M1}Al^{M2}(Al_xFe_{1-x})^{M3}Si_3O_{12}(OH), \quad (4)$$

such that x represents the mole fraction of Fe(III) in the M1 sites. Bird and Helgeson (1980) and Gottschalk (2004) represent the intracrystalline exchange reaction for Al and Fe(III) between the M1 and M3 sites within epidote by:

$$Fe(III)_{M3} + Al_{M1} = Fe(III)_{M1} + Al_{M3}, \quad (5)$$

such that:

$$\frac{X_{Fe,M1} \cdot X_{Al,M3}}{X_{Fe,M3} \cdot X_{Al,M1}} = K', \quad (6)$$

where K′ represents the "intracrystalline equilibrium constant" for reaction (5) [see Bird and Helgeson (1980) for intracrystalline standard state conventions adopted]. The values of K′ are computed for epidote solid solutions by the temperature-dependent relationship:

$$\log K' = -1523.4\left(\frac{1}{T}-\frac{1}{T_r}\right) - 5.0, \quad (7)$$

where T is the temperature of the system and T_r is the reference temperature of 298.15 K (25°C; Bird and Helgeson, 1980).

Assuming ideal mixing of Al and Fe(III) on the M1 and M3 sites, the thermodynamic activity of the clinozoisite ($Ca_2Al_3Si_3O_{12}(OH)$) component of epidote solid solutions can be computed by:

$$a_{czo} = X_{Al,M1} \cdot X_{Al,M3}, \quad (8)$$

where $X_{Al,M1}$ is the mole fraction of Al in the M1 site and $X_{Al,M3}$ is the mole fraction of Al in the M3 site (Bird and Helgeson, 1980).

Based on total measured Fe(III) content of epidote (n_{Fe}), equation (5) is rearranged to determine the distribution of the Al and Fe(III). Since:

$$X_{Fe,M1} = n_{Fe} - X_{Fe,M3}, \quad (9)$$

$$X_{Fe,M3} = n_{Fe} - X_{Fe,M1}, \quad (10)$$

$$X_{Al,M3} = 1 - X_{Fe,M3}, \quad (11)$$

and

$$X_{Al,M1} = 1 - X_{Fe,M1}, \quad (12)$$

equation (6) can be expressed in terms of the intracrystalline equation constant, K′ (eq 7), the measured total Fe(III), n_{Fe}, and the mole fraction of Fe(III) in the M3 site:

$$K'_{T,P} = \left(\frac{(n_{Fe} - X_{Fe,M3})(1 - X_{Fe,M3})}{X_{Fe,M3}(1 - (n_{Fe} - X_{Fe,M3}))}\right) \quad (13)$$

where n_{Fe} represents the total number of moles of Fe(III) per formula unit in the analyzed epidote. Equation (13) is reduced to the following quadratic equation:

$$0 = (1 - K') \cdot X^2_{Fe,M3} - (1 + n_{Fe} - K'(1 - n_{Fe})) \cdot X_{Fe,M3} + n_{Fe}. \quad (14)$$

Calculated values of $X_{Fe,M3}$ using equation (14) and measured n_{Fe} allows determination of $X_{Fe,M1}$, $X_{Al,M3}$, and $X_{Al,M1}$ using equations (9), (10), (11) and (12) and thus the calculation of a_{czo} by equation (8).

Calculations of thermodynamic activities of epidote solid solution components commonly assume that all Fe(III) preferentially substitutes into only the M3 site, the largest of the three octahedral sites (Dollase, 1971). Under this assumption, previous researchers (Giggenbach, 1981; Stefánsson and Arnórsson, 2002) have used the relationship:

$$a_{czo} = 1 - 3 \cdot X_{ps} \quad (15)$$

where X_{ps} is the mole fraction of Fe(III) in epidote (Bird and Helgeson, 1981). While this is an excellent approximation of a_{czo} for most epidotes, it fails to account for the Fe(III)-rich epidotes with an $X_{ps} > 0.33$; values of $X_{ps} > 0.33$ would result in the calculation of a negative value for a_{czo} using equation (15).

The activity of clinozoisite was computed for compositions of epidote reported in table A1 and figure 7 using equation (15) for ordered epidote (Al^{3+} in M3 site only) and equation (8) for equilibrium disordered epidote (Al^{3+} in both M1 and M3 sites). At $X_{ps} = \sim 0.3$, these two models for calculating a_{czo} deviate from one another, as shown in figure 9. The deviations from what should be a smooth distribution of points

using equation (8) is due to temperature effects on the calculation of the intracrystalline equilibrium constant, K′, from equation (7) where, in some cases, the same X_{ps} values are from samples of drill cuttings obtained at different temperatures.

Prehnite.—The activity of the $Ca_2Al(AlSi_3O_{10})(OH)_2$ component in Fe(III)-Al prehnite solid solutions used in equation (3) is computed with an ideal site mixing approximation of:

$$a_{\text{preh}} = X_{\text{Al,Prehnite}}, \tag{16}$$

where $X_{\text{Al,Prehnite}}$ is equal to the mole fraction of octahedral Al (Bird and Helgeson, 1980). As noted above, trace quantities of prehnite crystals were difficult to isolate in the drill cutting samples, so it was not possible to conduct extensive electron probe microanalysis as with the more modally abundant epidote. It was therefore necessary to calculate prehnite compositions by expressing Fe-prehnite compositions as a function of epidote Fe(III) and Al content, a thermodynamic constraint consistent with the phase rule analysis given above.

Equilibrium between coexisting epidote and prehnite solid solutions is represented by the reaction:

$$\underset{\text{epidote}}{Ca_2FeAl_2Si_3O_{12}(OH)} + \underset{\text{Al-prehnite}}{Ca_2Al(AlSi_3O_{10})(OH)_2} = \underset{\text{clinozoisite}}{Ca_2Al_3Si_3O_{12}(OH)} + \underset{\text{Fe-prehnite}}{Ca_2Fe(AlSi_3O_{10})(OH)_2}. \tag{17}$$

At equilibrium, the compositions of prehnites ($X_{\text{Al,Prehnite}}$) are determined by using the equilibrium constant, K'', for equation (17), and the activity ratio of the epidote (a_{epi}) to clinozoisite (a_{czo}) components in Al-Fe(III) epidote solid solutions by the relationship:

$$X_{\text{Al,Prehnite}} = \left(1 + K''_{T,P}\left[\frac{a_{epi}}{a_{czo}}\right]\right)^{-1}, \tag{18}$$

where a_{epi} is computed using equation (20) of Bird and Helgeson (1980), a_{czo} is computed from the relationship of equation (8) above, and $X_{\text{Al,Prehnite}}$ is the mole fraction of octahedral Al in Al-Fe(III) prehnite solid solutions (Bird and others, 1984). Using regression analysis on the observed compositional relations between coexisting epidote and prehnite solid solutions from the Cerro Prieto geothermal system in Mexico, Bird and others (1984) determined that a $K''_{T,P} = 10^{-1.27}$ provided the best fit curve proxy for the partitioning of Fe(III) and Al between epidote and prehnite in geothermal systems within the constraints of $X_{ps} = 0$, $X_{\text{Fe,Prehnite}} = 0$ and $X_{ps} = 0.33$, $X_{\text{Fe,Prehnite}} = 1.0$.

The Bird and others (1984) model, however, precludes the use of epidotes with $X_{ps} > 0.33$ because it assumes Fe(III) substitution only in the M3 crystal site by defining a_{czo} by equation (15). Therefore, in order to determine a relationship between epidote and prehnite compositions that is not limited to $X_{ps} < 0.33$, a sigmoidal regression was employed to fit a data set consisting of the coexisting epidote and prehnite compositions from active geothermal systems reported by Bird and others (1984) and Milodowski and others (1989), together with compositional constraints from mineral analyses of drill cuttings from the Reykjanes geothermal system reported by Lonker and others (1993), Marks and others (personal communication/2006), and the present study (see fig. 10 for details). The regression is subject to the compositional constraints that epidote with $X_{ps} = 0$ coexists with prehnite of $X_{\text{Fe,Prehnite}} = 0$, and that the most Fe(III)-rich epidote ($X_{ps} = 0.36$) found in cuttings where we have also analyzed prehnite (RN-17, 700 and 800 m depth) coexists with the most Fe(III)-rich prehnite

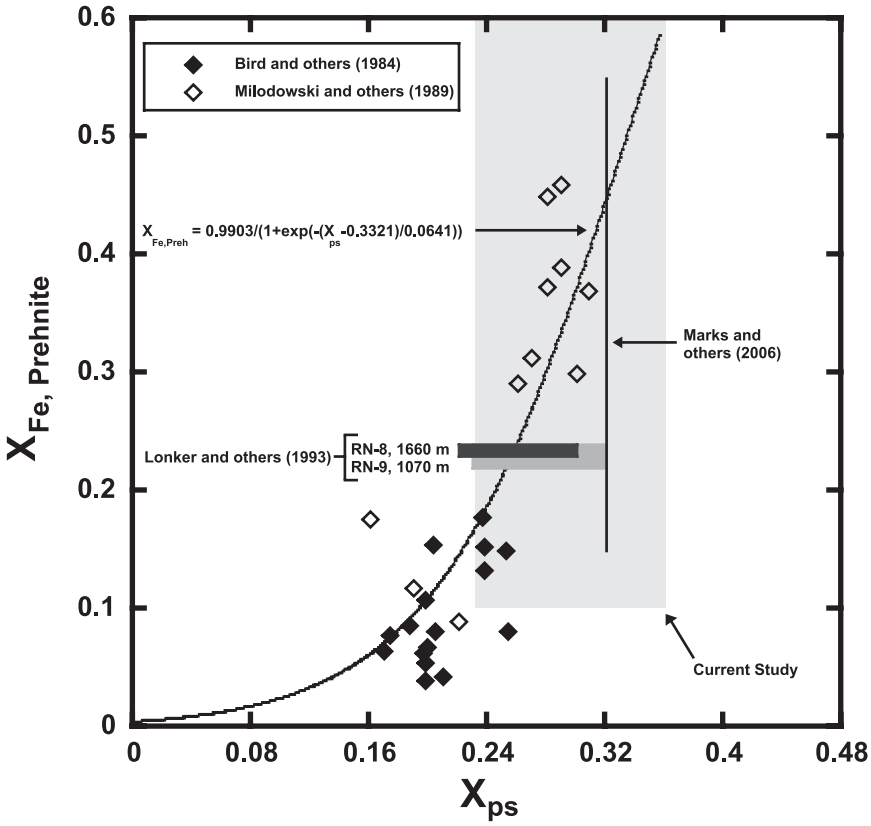

Fig. 10. Compositional relations of Fe(III)-Al partitioning between epidote (X_{ps}) and prehnite ($X_{Fe,Prehnite}$) in the Cerro Prieto geothermal system, Mexico (Bird and others, 1984), Miravalles geothermal system, Costa Rica (Milodowski and others, 1989), and the Reykjanes geothermal system, Iceland (ranges of compositions reported by Lonker and others, 1993; Marks personal communication; Marks and others, 2006; and present study). The black curve denotes compositional relations consistent with equation (20). (See text for details).

($X_{Fe,Prehnite}$ = 0.60) found at the same depths (this study; see figs. 7, 8 and 10, and tables A1 and A3 of the Appendix). The computed compositional relationship between X_{ps} and $X_{Fe,Prehnite}$ is:

$$X_{Fe,Prehnite} = 0.9903/(1 + \exp(-(X_{ps} - 0.3321)/0.0641)) \quad (19)$$

(fig. 10). Since Fe(III) substitutes for Al in one octahedral site of prehnite, then:

$$X_{Al,Prehnite} = 1 - X_{Fe,Prehnite}$$
$$= 1 - (0.9903/(1 + \exp(-(X_{ps} - 0.3321)/0.0641))). \quad (20)$$

Compositions of prehnite computed using equation (20) and the measured compositions of epidote (table A1 and fig. 7) are shown in figure 8 as a function of depth. Both the calculated and measured prehnite compositions represent similar values and ranges of Al and Fe, providing some degree of confidence in the use of calculated prehnite compositions in evaluating equilibrium for reaction (1). Thus, using equations (16) and (20) to calculate $X_{Al,Prehnite}$ values for every epidote analysis ($X_{ps} < 0.36$) enables the calculation of a_{preh} for each theoretically coexisting prehnite

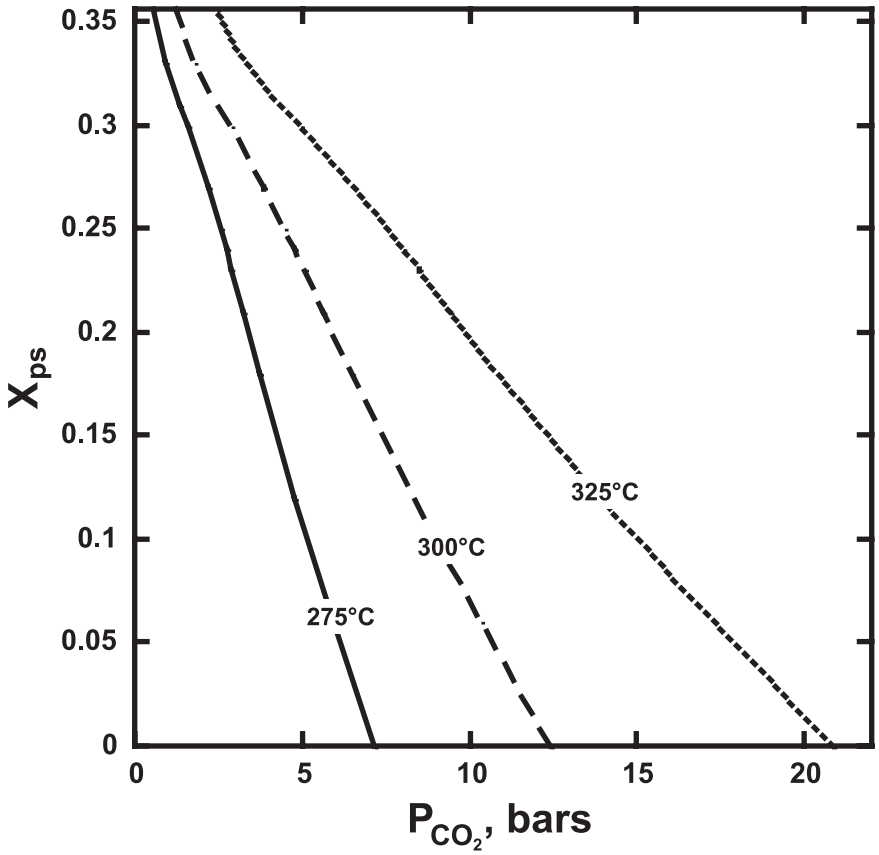

Fig. 11. Compositional constraints between epidote composition (X_{ps}) and the partial pressure of $CO_{2,g}$ at 275°, 300° and 325°C required by equilibrium for reaction (1) and equations (3) and (20). The sigmoid nature of the curves is an artifact of the regression of the data in figure 10 (eq 19). (See text for details).

crystal. Employing this approach for determining prehnite composition, the calculated $X_{Fe,Prehnite}$ values using compositional data of epidote from table A1 are graphically illustrated in figure 8, where it can be seen that predicted prehnite compositions range from ~0.05 to 0.6.

Equilibrium Constraints on P_{CO_2}

Equations and data presented above permit calculation of the partial pressure of CO_2 from equation (3) as a function of epidote composition at constant temperature, pressure and activity of H_2O (equal to 0.985) for equilibrium among epidote-prehnite-calcite-quartz and fluid (reaction 1). In equation (3) the activity of the Al-prehnite component (a_{preh}) is computed using equations (16) and (20) as described above. The results are shown in figure 11 at constant temperatures of 275°, 300° and 325°C for pressures equal to liquid-vapor equilibrium of H_2O. It is apparent from the diagram that equilibrium constraints imposed by reaction (1) requires that P_{CO_2} increases with decreasing X_{ps} at constant temperature, and at constant X_{ps}, P_{CO_2} increases with increasing temperature, but to a lesser degree with increasing Fe(III) content in epidote. Inflections in the curvature of the isopleths in figure 11 are an artifact of the

sigmoidal regression of the data in figure 10 and the temperature dependence of substitutional order-disorder in epidote solid solutions.

CALCULATION OF AQUIFER FLUID COMPOSITION

In this section we report new values for partial pressures of CO_2 in the Reykjanes geothermal system and summarize procedures and assumptions adopted for deriving partial pressures of CO_2 in well discharge fluids for correlation with values of P_{CO_2} predicted from the local equilibria for reaction (1) and mineralogic phase relations in wells RN-9, RN-9 and RN-17. Finally, in order to quantify the extent to which local equilibrium among the assemblage epidote-prehnite-calcite-quartz and fluid occurs in the Reykjanes geothermal system we assess the saturation state for individual minerals in the assemblage using aqueous speciation computations together with equilibrium constants for hydrolysis and solubility reactions.

Calculation Procedure

As previously noted, measured temperatures in thermally stabilized wells in the central part of the Reykjanes geothermal field to depths of ~1000 to 1400 m closely approximate the temperature-depth relationships for liquid-vapor equilibrium for aqueous solutions of seawater compositions (based on the 1997 IAPWS Industrial Formulation for thermodynamic properties of water and steam; see Arnórsson and others, 2007). Until the commission of the new 100 MWe power plant in May 2006, the discharge enthalpy of the wells at Reykjanes was similar to that of steam-saturated water at the temperature of producing horizons. The enthalpy of production wells at Reykjanes has now increased as a result of geothermal fluid pressure drop due to power production. In this study we consider only fluid samples that were collected before significant drawdown in the system affected production fluid enthalpy. In addition, concentrations of individually analyzed solute components in the unboiled aquifer fluid have been derived from analytical data on liquid and vapor samples collected at the wellhead using a Webre separator. The composition of the reservoir liquid is computed from analyses of the liquid and the vapor fraction using the following mass balance equation:

$$m_i^{f,l} = m_i^{d,l}(1 - X^d) + m_i^{d,v}X^d, \tag{21}$$

where m denotes concentration and subscript i denotes component i. Superscript f,l designates the unboiled deep geothermal fluid and d,l and d,v refer to the liquid and vapor samples, respectively, collected at the wellhead. X^d is the vapor fraction of the discharge at sampling conditions, and $(1 - X^d)$ is therefore the liquid fraction. For dissolved solids the value of $m_i^{d,v}$ was taken to be zero, that is, these components partition insignificantly into the vapor phase at sampling conditions. Similarly, $m_i^{d,l}$ for the less liquid soluble gases (H_2, CH_4, N_2, Ar, *et cetera*) was also taken to be zero. Total carbonate carbon, total sulfide sulfur, NH_3, and B were determined in both types of samples collected to obtain their concentration in the un-boiled deep aquifer liquid water. The acid gases (CO_2 and H_2S) in the vapor samples constitute most of these components in the total well discharge. The value of X^d was obtained from

$$X^d = \frac{h^{f,l} - h^{d,l}}{h^{d,v} - h^{d,l}} \tag{22}$$

taking the discharge enthalpy ($h^{f,l}$) to be equal to the enthalpy of vapor saturated liquid at the selected aquifer temperature ($h^{f,l}$). The superscripts in equation (22) have the same notation as in equation (21). The values for $h^{d,l}$ and $h^{d,v}$ are known as both temperature and pressure in the separator are measured during sampling. It is a good approximation to assume liquid enthalpy for fluid samples collected before

mid-year 2006 in Reykjanes wells. This approximation is also reasonably good for excess enthalpy wells if the excess enthalpy of the well discharge is caused by phase segregation in the producing aquifers, which involves flow of all the steam into the well but partial retention of the liquid water because of its adhesion onto mineral surfaces due to capillary forces (see Arnórsson and others, 2007 for detailed discussion). The computed deep fluid concentration is sensitive to the enthalpy of the un-boiled fluid, $h^{f,1}$, assigned to individual wells. Here we assume that the enthalpy or reference temperature is constant over time. The reference temperatures for the wells considered in this study, and reported in tables 1 and 2, were determined by careful consideration of available temperature logs from the wells and the concentration of dissolved silica in available fluid samples assuming equilibrium with quartz (Fridriksson and Giroud, 2008).

Having obtained the concentration of $CO_{2,aq}$ in the un-boiled aquifer fluid with the aid of equations (21) and (22), the partial pressure of CO_2 was derived from the calculated concentration of dissolved CO_2 in the initial un-boiled aquifer liquid using the CO_2 solubility constant in the thermodynamic database in the computer program WATCH (fit through data tabulated by Naumov and others, 1971; see Arnórsson and others, 1982). Use of more recent data on CO_2 solubility in water (Fernandez-Prini and others, 2003) yields essentially identical results. The calculated CO_2 partial pressure below the depth level of first boiling is not sensitive to the calculated pH of the aquifer liquid water because almost all the carbonate carbon (>90%) occurs as CO_2. The parameters that affect the calculated CO_2 concentration in the aquifer water and CO_2 partial pressures mostly are analytical inaccuracy of CO_2 concentrations in vapor samples and the vapor fraction of the well discharge at sampling conditions as determined by the recorded sampling pressure and the selected aquifer temperature. The overall error is estimated as <10 percent.

Most modern geothermal fluid analyses for this study come from the Iceland GeoSurvey database, where the WATCH computer program (Arnórsson and others, 1982), version WDENS23 (Bjarnason, 1994) was used to compute the composition and aqueous speciation of the deep fluid. Calculated P_{CO_2} from geothermal fluid analyses shown in table 2 are between 1.3 and 4.0 bars at reference temperatures between 275 and 310°C.

Alternate values of deep fluid P_{CO_2} from the Reykjanes geothermal systems were computed for five chemical analyses from the Iceland GeoSurvey database from wells RN-10, RN-12, RN-19, RN-21, and RN-23 (table 1) using the SOLVEQ and CHIM-XPT codes (formerly CHILLER; Reed, 1982). The modeling of the deep fluid composition involved correction of the fluid composition to account for precipitation of sphalerite and chalcopyrite during fluid ascent in the well (see for example, Akaku and others, 1991), because these sulfides are known to form scales in production wells at Reykjanes (Hardardóttir and others, 2005). The sulfide precipitation corrections increase the concentrations of Zn and Cu in the deep fluid significantly. The effect on pH was small for the three cooler samples (0.02 to 0.05) but moderate in the two hottest samples (0.11 to 0.17). The corrections also had a minor effect on the concentration of sulfide and sulfate in the deep geothermal fluid. Estimated uncertainty of the resulting pH values are not considered to be larger than $+/-0.3$. At reference temperatures of 275°, 285°, 295° 300° and 310°C the values of P_{CO_2} are 1.41, 1.50, 2.42, 1.54, and 2.34, respectively (table 1). These values are slightly lower than values for the same samples reported in table 2 because the speciation calculations using the WATCH program result in somewhat lower pH values for the deep fluid and will thus tend to overestimate the fraction of the total dissolved carbonate that occurs as $CO_{2,aq}$ relative to the speciation calculations and sulfide correction using SOLVEQ and CHIM-XPT.

TABLE 2

Summary of geothermal fluid P_{CO_2} values from the Reykjanes Geothermal System derived from analytical data on liquid and vapor samples collected at the surface from wet-steam well discharges using the WATCH speciation program

Well	Ref T (°C)	Fluid P_{CO_2}	Well	Ref T (°C)	Fluid P_{CO_2}
RN-8	275	3.43	RN-9	295	2.39
RN-8	275	2.33	RN-9	295	2.17
RN-8	275	2.65	RN-9	285	2.60
RN-8	275	2.48	RN-9	285	2.48
RN-8	275	3.78	RN-9	285	1.53
RN-8	275	2.36	RN-10	285	1.64
RN-8	275	2.86	RN-10	275	1.60
RN-8	275	2.19	RN-10	275	1.30
RN-8	275	2.98	RN-10	285	1.61
RN-8	275	1.57	RN-10	285	1.85
RN-8	275	1.95	RN-11	300	1.76
RN-8	275	1.78	RN-11	300	2.30
RN-8	275	1.70	RN-12	300	1.72
RN-8	275	1.78	RN-12	300	2.11
RN-9	290	1.75	RN-12	285	1.97
RN-9	290	1.75	RN-12	285	2.22
RN-9	290	1.84	RN-12	290	1.97
RN-9	290	1.90	RN-12	290	1.87
RN-9	290	1.75	RN-12	290	1.68
RN-9	290	1.82	RN-15	290	2.28
RN-9	290	1.78	RN-15	290	2.14
RN-9	290	1.90	RN-18	310	2.87
RN-9	290	2.06	RN-18	310	2.60
RN-9	290	1.73	RN-19	310	2.42
RN-9	290	1.82	RN-19	310	2.94
RN-9	290	2.14	RN-21	310	4.04
RN-9	290	1.75	RN-21	295	2.76
RN-9	290	1.71	RN-22	295	3.04
RN-9	290	1.80	RN-22	295	2.70
RN-9	290	1.83	RN-23	295	2.17
RN-9	290	1.70	RN-23	295	2.34
RN-9	290	1.93	RN-24	295	2.50
RN-9	290	2.08	RN-24	295	2.33
RN-9	290	1.74	*RN-9	295	2.59
RN-9	290	2.54	*RN-9	295	2.30
RN-9	290	2.50			

All fluid concentrations reported in bars.

All fluid data from Iceland GeoSurvey database, except: *Lonker and others (1993).

Fluid P_{CO_2} calculated using the aqueous speciation computer program WATCH (Arnórsson and others, 1982), version 2.1 (Bjarmason, 1994).

EVALUATION OF LOCAL EQUILIBRIUM

Thermodynamic activities of aqueous species computed with the SOLVEQ and CHIM-XPT (Reed, 1982) computer programs for geothermal fluids reported in table 1 are used to evaluate the extent to which the hydrothermal solutions are in equilibrium with the mineral assemblage epidote, prehnite, calcite and quartz (see for example, reaction 1). Fluid samples analyzed by SOLVEQ and CHIM-XPT were chosen from wells at different temperatures that demonstrated excellent charge balance and were collected after well testing, so that enough discharge had already occurred to indicate that primary formation fluids were being produced from the drillhole. In addition, samples collected before June 2006 were chosen for analysis, as drawdown in the system increased the steam fraction in the wells, making the gas composition less reliable. Equilibrium constants used in the solubility calculations presented below are from the SOLVEQ program, which employs the thermodynamic properties of minerals from Holland and Powell (1998), and for aqueous species from the SLOP98 data base [the SLOP98 database is based on the SPRONS92 database (Johnson and others, 1992) with later additions by Everett Shock and coworkers (http://geopig.asu.edu/supcrt92_data/slop98.dat)]. The computed activity of H_2O used in these and subsequent calculations is 0.985 (see table 1).

The geothermal fluids reported in table 1 are close to demonstrating equilibrium with quartz, as illustrated in figure 12A, where the symbols denote the activities of aqueous silica in the geothermal fluids and the solid line is the equilibrium constant for the quartz solubility reaction ($SiO_{2,quartz} \leftrightarrow SiO_{2,aq}$). We note that the geothermal fluids are slightly supersaturated with respect to quartz in accordance with the experimental results presented by Fournier (1983), which describes the effect of salinity on quartz solubility, an effect not accounted for in the computer program SOLVEQ.

Evaluation of the degree to which geothermal fluids reported in table 1 are in equilibrium with calcite, epidote and prehnite (using the end-member components specified in reaction 1) requires values of the thermodynamic activities of Ca^{2+}, Al^{3+} and $CO_{2,g}$, in addition to that for $SiO_{2,aq}$ and H^+. We note that the concentration of $SiO_{2,aq}$ is close to equilibrium with quartz (fig. 12A), and that the maximum error for solution pH is approximately $+/-0.3$ (see above). However, it is difficult to characterize possible errors in the thermodynamic activities of Ca^{2+}, Al^{3+} and HCO_3^- derived from speciation computations of the geothermal fluids with near seawater salinities. An alternate calculation of the saturation state of anhydrite provides some indication of the validity of our computed activities of Ca^{2+}. Anhydrite is a common hydrothermal mineral in the lower portions of the chlorite-epidote zone (fig. 3; Lonker and others, 1993; Franzson and others, 2002; Fridleifsson and others, 2005). The equilibrium constant for the reaction

$$\underset{Anhydrite}{CaSO_4} = Ca^{2+} + SO_4^{2-} \tag{23}$$

is shown in figure 12B as a function of temperature at pressures equal to liquid-vapor equilibrium for H_2O. Symbols in the figure denote the ion activity product ($Q_{anhydrite}$) for reaction (23),

$$\log Q_{anhydrite} = \log (a_{Ca^{2+}} \cdot a_{SO_4^{2-}}). \tag{24}$$

Close correlation between the equilibrium constant (solid line) and values of the ion activity products (symbols) in figure 12B suggest equilibrium between the geothermal fluids and anhydrite. Thus, errors in our computed values for the thermodynamic activity of aqueous Ca^{2+} are likely not significant.

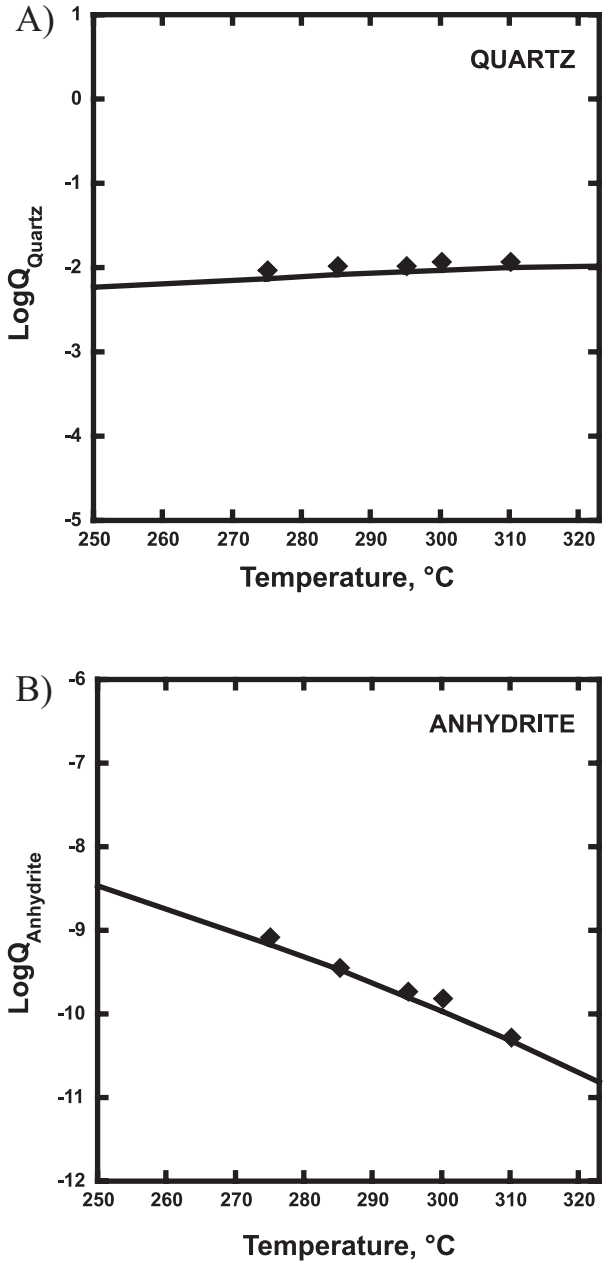

Fig. 12. Saturation conditions for (A) quartz and (B) anhydrite in the Reykjanes geothermal system based on distribution of aqueous species in geothermal fluids reported in table 1 (see text for details). Solid lines denote values of the equilibrium constant for the dissolution reactions and the symbols denote values of the molality of aqueous silica (represented as Log $m_{SiO_2,aq}$ = Log Q_{quartz}; fig. 12A) and the value the ion activity product for reaction (23), as represented by equation (24).

The saturation state of calcite, epidote and prehnite in the Reykjanes geothermal system is evaluated by employing the methodology represented in figure 12 for quartz and anhydrite using the following hydrolysis reactions:

$$\underset{calcite}{CaCO_3} + 2H^+ = Ca^{2+} + H_2O, + CO_{2,g} \quad (25)$$

$$\underset{clinozoisite}{Ca_2Al_3Si_3O_{12}(OH)} + 13\ H^+ = 2\ Ca^{2+} + 3\ Al^{3+} + 3\ SiO_{2,aq} + 7\ H_2O, \quad (26)$$

and

$$\underset{prehnite}{Ca_2Al_2Si_3O_{10}(OH)_2} + 10\ H^+ = 2\ Ca^{2+} + 2\ Al^{3+} + 3\ SiO_{2,aq} + 6\ H_2O. \quad (27)$$

Values of the logarithm of the equilibrium constant for reaction (25), (26) and (27) are shown as solid lines in figure 13 as a function of temperature (for pressures of liquid-vapor equilibrium of H_2O). Symbols in the figure denote the ion activity products for geothermal fluids reported in table 1 and defined by:

$$\log Q_j = \sum_i \log a_i^{v_i}, \quad (28)$$

where Q_j is the ion activity product of mineral component j [that is, the $Ca_2Al_3Si_3O_{12}(OH)$ component in Fe(III)-Al epidote solid solutions for reaction 26, and the $Ca_2Al_2Si_3O_{10}(OH)_2$ component of Fe(III)-Al prehnite solid solutions for reaction 27], and a_i and v_i are, respectively, the thermodynamic activity and stoichiometric reaction coefficient (positive for products and negative for reactants) of the i^{th} aqueous species in reaction (25) thru (27). Values of log Q_i for geothermal fluids reported in table 1 are represented by the diamond symbols in figure 13. Error bars in the figure represent the assumed cumulative error of $+/-0.3$ in pH, but do not account for the <10 percent assumed error in values of P_{CO_2} reported in tables 1 and 2 (compare fig. 13A). Dashed lines in figures 13B and 13C denote values of the equilibrium constant for reactions (26) and (27) that account for compositional variation of octahedral substitutions of Fe(III) and Al in the minerals epidote and prehnite, mathematically represented by the equilibrium constant relationship for chemical reactions (compare Krauskopf and Bird, 1995).

The ion activity products for calcite (reaction 25) shown in figure 13A indicate, within the upper limits of our assumed uncertainty in pH of $+/-0.3$, that calcite is in equilibrium with the geothermal fluids (solid diamonds in the figure denote values of P_{CO_2} reported in table 1 and the gray rectangles represent the range in values reported in table 2). We note that the error bars in the figure do not account for the <10 percent error we assume for the values of P_{CO_2} reported in tables 1 and 2 that are used in the calculation of $Q_{calcite}$. Following similar analyses as described above, Lonker and others (1993) report that fluids from well RN-8 (270°C) are slightly supersaturated with respect to calcite, and those from well RN-9 (295°C) are slightly undersaturated. Arnórsson (1978) and Arnórsson and others (1978, 1983) similarly conclude that calcite is supersaturated in fluids from well RN-8. However, Reed and Spycher (1984), using fluid analyses reported by Arnórsson and others (1983), report calculations indicating undersaturation with respect to calcite in the same drillhole. As noted by Lonker and others (1993) there is likely to be a notable uncertainty in evaluating the saturation state of Reykjanes geothermal fluids with respect to calcite because of the sensitive dependence on analyses of well discharge and on interrelated computations of solution pH, total dissolved carbonate and partial pressures of CO_2 for fluids with seawater salinity. Taken together, the geothermal fluids at Reykjanes are considered to be close to saturation with respect to calcite, and at most are only slightly undersaturated within the temperature range of 275° to ~310°C.

It is apparent that geothermal fluids reported in table 1 are in equilibrium with epidote and prehnite over the observed compositional range of these minerals in the

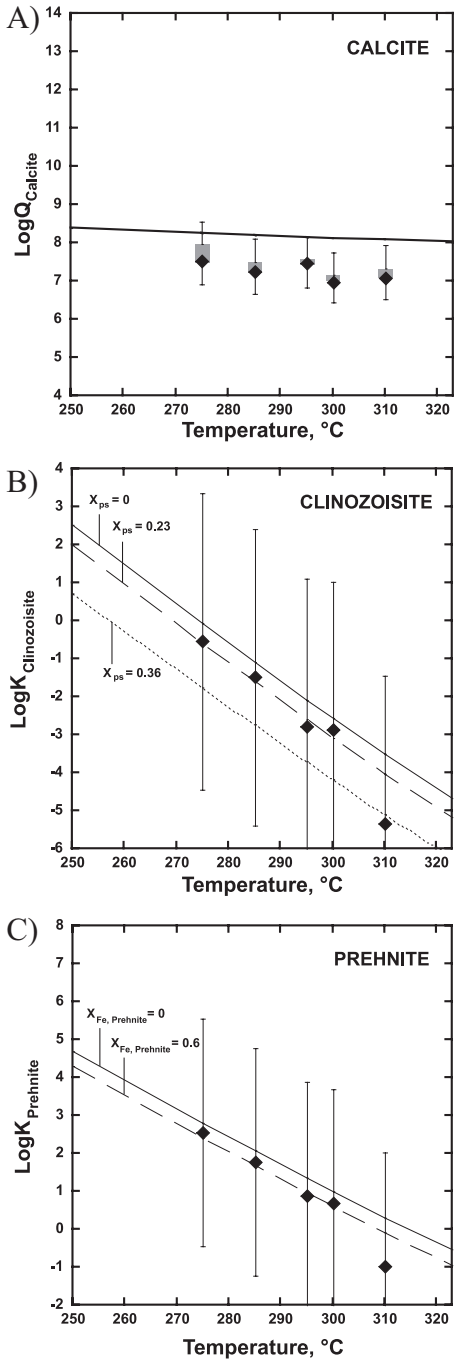

Fig. 13. Saturation conditions for (A) calcite, (B) clinozoisite and (C) prehnite in the Reykjanes geothermal system based on the distribution of aqueous species for geothermal fluids reported in table 1 (see text for details). Solid lines represent values of the equilibrium constant as a function of temperature for reactions (25), (26) and (27) and the symbols denote values of the ion activity products for these reactions (eq 28). Error bars denote +/− 0.3 pH units. Broken lines in diagrams (B) and (C) denote isopleths for the noted compositions of epidote and prehnite solid solutions.

Reykjanes geothermal system (figs. 13B and C). Considering our adopted uncertainty in pH of +/−0.3, all of the ion activity products shown in figures 13B and C are consistent with equilibrium of the geothermal fluids with epidote and prehnite. These observations are in accord with Sveinbjörnsdóttir (1983, 1992) and Ragnarsdóttir and others (1984) who conclude that the hydrothermal minerals approached equilibrium with the Reykjanes geothermal fluids.

Reed and Spycher (1984) predict that epidote is saturated in geothermal fluids from well RN-8, as do Lonker and others (1993) for both RN-8 and RN-9. However, Lonker and others (1993) suggest that the observed compositions of prehnite are not stable at the Reykjanes reservoir temperatures and values of the activity ratios of Ca^{2+} to H^+. We note from their figure 16 that they predict a mole fraction of the Fe(III) component ($X_{Fe,Prehnite}$) of <0.05 to be in equilibrium with Fe(III)-rich epidote. This value is inconsistent with the ion activity products and equilibrium constants relationship shown in figure 13C, which indicate saturation of the Reykjanes geothermal fluids with prehnite over the temperature range of 275° to 310°C, and with the compositional relations of Fe(III)-Al partitioning illustrated in figure 10 (eq 20), which is consistent with values of coexisting epidote and prehnite they report from RN-8 and RN-9 (see fig. 16 of Lonker and others, 1993, and symbols in fig. 10 representing their data).

Correlation of fluid P_{CO_2} values derived from mineralogical phase relationships and geothermal discharge fluids

Equations and data presented above permit calculation of the partial pressure of CO_2 from equation (3) as a function of the measured epidote compositions reported in table A1 of the Appendix and figure 7 (only values of $X_{ps} < 0.36$ were employed in this study, per the compositional constraints defined in fig. 10) at constant temperature, pressure and activity of H_2O (equal to 0.985, see table 1) for equilibrium among epidote-prehnite-calcite-quartz and fluid (reaction 1). In equation (3) the activity of the Al-prehnite component (a_{preh}) is computed using equations (16) and (20) (see fig. 10).

For all calculated P_{CO_2} values in the upper 1400 m of the system, the boiling point curve of seawater serves as a proxy for the original well temperatures at depth during mineral paragenesis, as the curve closely approximates downhole temperatures within the localized upflow zone in well RN-10, just above the approximated temperature of first boiling for seawater of 320°C (Franzson and others, 2002; Arnórsson and others, 2007). Below this depth, temperatures remain relatively uniform, consistent with convectional heat flow in a one-phase system. Given the uniformity of mineral zone depths in wells RN-17 and RN-9 relative to that of RN-10 (fig. 3), it is likely that peak temperatures throughout the geothermally active region were similar to the temperature gradient observed in well RN-10 today. Therefore, epidote-formation temperatures adopted in this study are approximated from the boiling point curve for seawater with depth up to 320°C and remain constant for samples collected below a depth of 1400 m (based on the 1997 IAPWS Industrial Formulation for thermodynamic properties of water and steam; see Arnórsson and others, 2007).

The results of our calculations are shown in figure 14 for the range in reference temperatures of 275° to 310°C, which corresponds to the temperatures of fluid analyses reported in tables 1 and 2. In figure 14, values of P_{CO_2} predicted from measured epidote compositions (diamonds) can be compared with values of P_{CO_2} reported in tables 1 and 2 as deduced from drillhole discharge fluids (squares in fig. 14A, and shaded area in fig. 14B). Predicted fluid P_{CO_2} values using epidotes from cuttings where the aggregate assemblage of epidote, prehnite, calcite and quartz is observed range from 0.57 to 6.17 bars. Predicted values from cuttings where calcite and/or prehnite are absent from the assemblage range from 1.32 to 6.81 bars. The histograms of figure 15 graphically represent the data presented in figure 14 over the

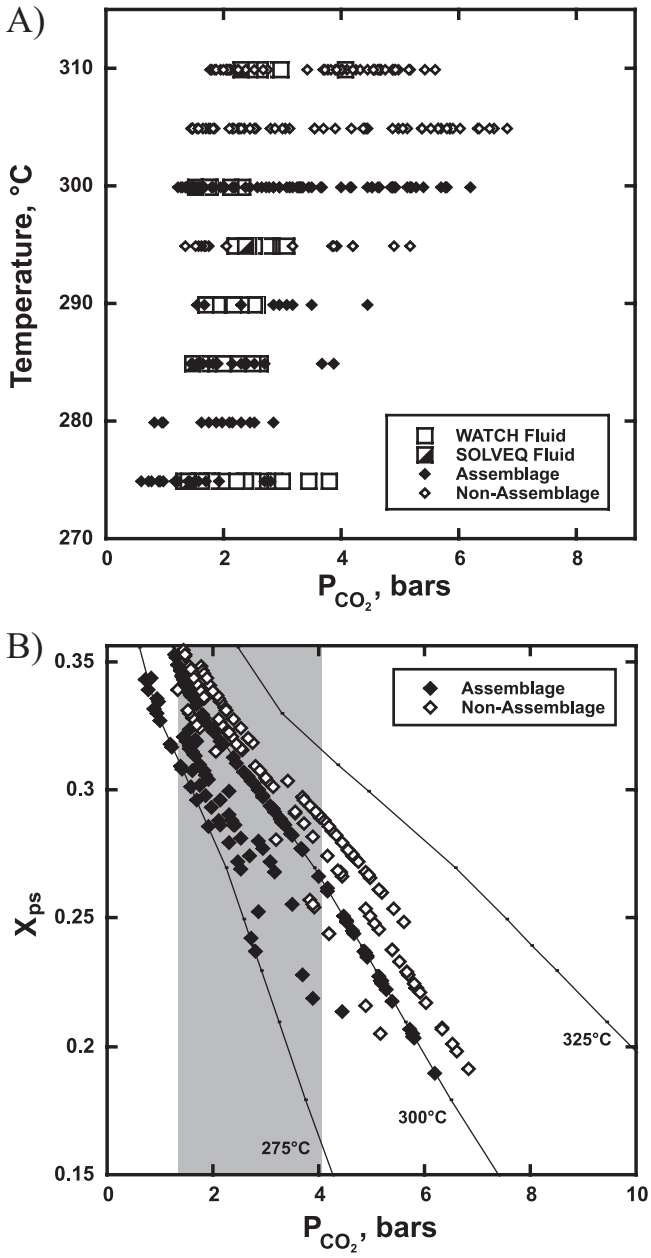

Fig. 14. Compilation of: 1) calculated CO_2 partial pressures (diamonds) consistent with equilibrium for reaction (1), epidote and prehnite compositions reported in figures 7 and 8 and equations, data and assumptions presented in the text, and 2) partial pressures of CO_2 reported in tables 1 and 2 determined from drillhole discharge fluids (squares; see text for details) as a function of reference temperature in diagram (A) and measured epidote compositions from wells RN-9, RN-10 and RN-17 in diagram (B). For definition of "assemblage" and "non-assemblage" see figure 8 caption. Solid lines in diagram (B) are from figure 11, and the shaded rectangle corresponds to the range in P_{CO_2} values reported in tables 1 and 2.

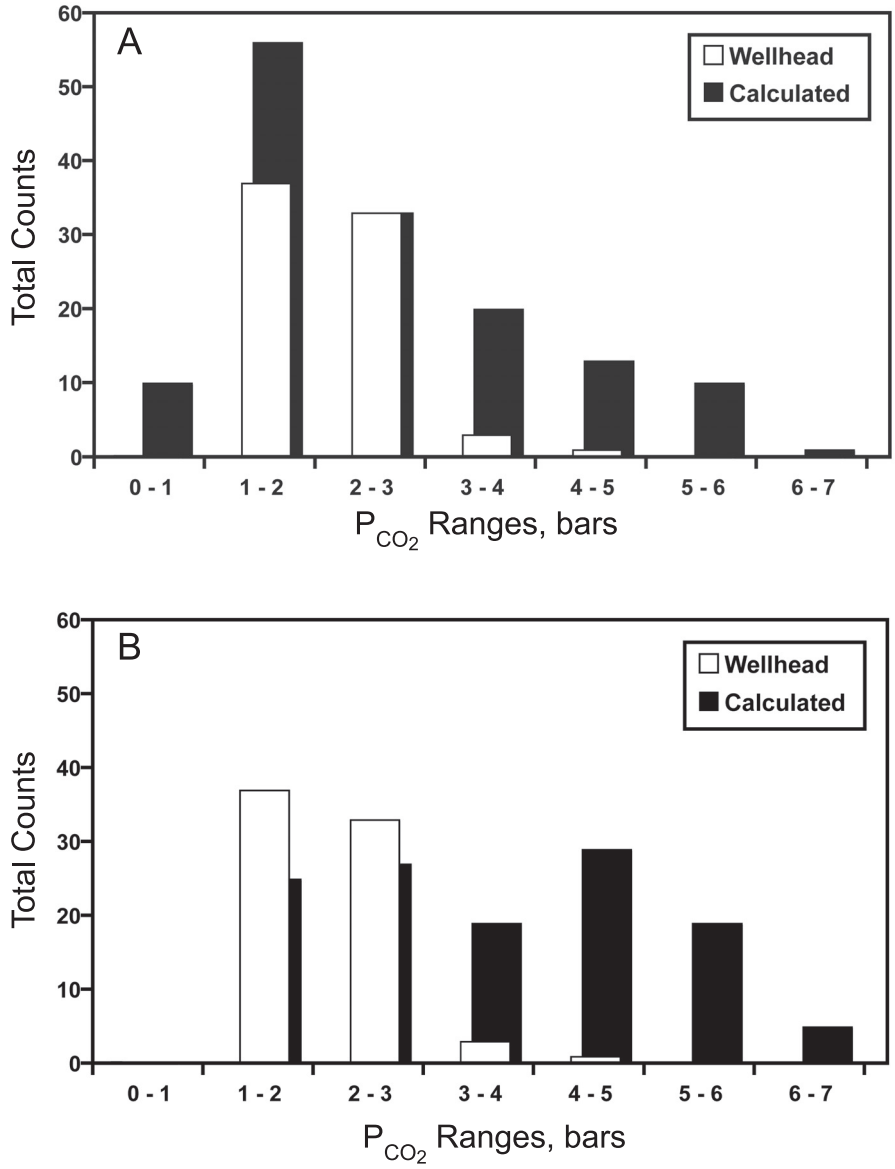

Fig. 15. The partial pressures of CO_2 presented in figure 14 represented as histograms of the number of analyses for: 1) calculated CO_2 partial pressures consistent with equilibrium for reaction (1), epidote and prehnite compositions reported in figures 7 and 8 and computed using equation (3) (black), and 2) partial pressures of CO_2 reported in tables 1 and 2 determined from drillhole discharge fluids collected at the wellhead (white). Diagram (A) presents values of calculated partial pressures of CO_2 based on measured epidote compositions from drillhole cuttings containing the assemblage epidote, prehnite, calcite and quartz (see figs. 3 and 7), and diagram (B) for measured epidote compositions where either prehnite or calcite was not observed (see text for details).

combined temperature range of 275° to 310°C; figure 15A illustrates 143 epidote analyses from cuttings with the aggregate assemblage (table A1, dark gray rows; figs. 3 and 7, depths with gray stippled bars) over the temperature range of 275° to 310°C (black bars; labeled "calculated" in the legend) compared with 74 computed P_{CO_2}

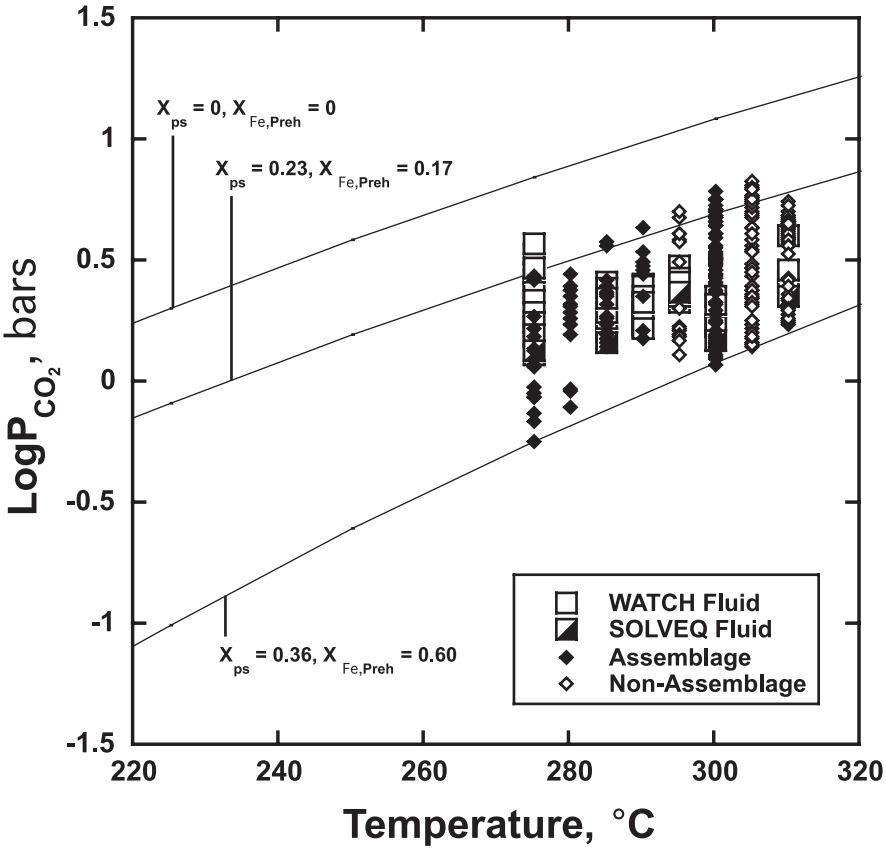

Fig. 16. Partial pressure of CO_2 as a function of temperature. Solid curves denote isopleths of equilibrium among epidote, prehnite, calcite, quartz and fluid ($a_{H_2O} = 0.985$) consistent with reaction (1) and equation (3) for the specified compositions of coexisting epidote and prehnite solid solutions (see text for details). Diamonds are values of P_{CO_2} computed from analyzed epidote compositions (see figs. 8 and 11 captions, and text for details), and the squares denote values of P_{CO_2} reported.

values from geothermal fluids (tables 1 and 2; white bars labeled "wellhead" in the legend). Figure 15B illustrates the same for 124 epidote compositions (table A1, light gray rows) where either prehnite or calcite was not observed in the drill cuttings (figs. 3 and 7, depths without gray stippled bars).

Finally, figure 16 shows the temperature dependence of the logarithm of P_{CO_2} for values computed for all epidote compositions reported in table A1 (where $X_{ps} < 0.36$) over the reference temperature range. In this figure the curves denote isopleths of the logarithm of P_{CO_2} as a function of temperature, which are consistent with equilibrium for reaction (1) and represented by equation (3) at various compositions of epidote and prehnite solid solutions; the diamonds are predicted values of logarithm of P_{CO_2} based on measured compositions of epidote and the squares are fluid analyses (tables 1 and 2).

DISCUSSION

Hydrothermal mineral paragenesis in geothermal environments is a function of the physical and chemical processes that characterize magma-hydrothermal systems. Intrusion of magmas into upper levels of the Earth's crust generates potentials for

irreversible transport of mass and energy (Norton, 1977, 1984; Cathles, 1977; Cathles and others, 1997). Heat transfer, fracture formation, fluid flow, and fluid-rock reaction are not independent processes, but related to one another through a series of intricate couplings (feedback loops) as described by Norton (1987, 1988, 1990) and Bredehoeft and Norton (1990). Potentials for irreversible reactions between hydrothermal solutions and their mineralogic environment are developed as fluids flow along variable temperature-pressure paths and encounter rocks of differing composition (Norton, 1979). Extrema in the thermodynamic and transport properties of water in the near critical region of H_2O has an important influence on advective transport rates of thermal energy and chemical components, as well as on the thermodynamic properties of aqueous electrolyte solutions, and thus, water-rock reaction (Helgeson, 1981; Norton, 1984; Johnson and Norton, 1991). Numerical experiments of heat and mass transfer in magma-hydrothermal systems reported by Norton and Dutrow (2001) demonstrate temporal oscillatory and chaotic variations in the transport and thermodynamic properties of aqueous solutions in the near critical region of water, and the resonant effect of these variations on chemical reactions (for example, oscillatory zoning in minerals, compare fig. 5A) and on fracture propagation. Coupled with a geologic history of multiple intrusions and related brittle deformation, as well as processes of boiling and mixing of fluids from different sources (that is, magmatic water, meteoric water, seawater, metamorphic water; Giggenbach and Stewart, 1982; Henley and Ellis, 1983; Hedenquest and others, 1992; Simmons and Christenson, 1994), the evolution of hydrothermal solutions and the paragenesis of secondary minerals represents the synergy of numerous complex processes. Oscillatory mineral deposition and replacement is likely due to the combined consequences of factors determining elemental mass transfer including diffusion, precipitation/dissolution kinetics, permeability changes (fracturing and fracture sealing), and multiple intrusion of magma into the heat source.

As a consequence of irreversible processes governing the dynamic nature of magma-hydrothermal systems one would *not* expect fluid-mineral equilibria to be attained in active geothermal systems. However, it was recognized during geothermal energy development in the 1960's that concentrations of aqueous silica, and alkali and alkaline earth cations in geothermal fluids (from both drillhole discharge fluids and natural surface discharges, such as hot springs) systematically correlated with subsurface temperatures, thus providing a basis for solute geothermometers useful for geothermal exploration that are broadly consistent with solution-mineral equilibria (compare Arnórsson, 1970, 1975, 1985; Fournier, 1973, 1977; Fournier and Truesdell, 1973; Fournier and Rowe, 1977; Fournier and Potter, 1979, 1982; Arnórsson and others, 1983). These relationships provide empirical evidence that many high-temperature geothermal fluids ($\gtrsim$200°C) approach equilibrium with secondary quartz, feldspars and calc-silicates, despite theoretical inferences of irreversible transport phenomena and reaction, as well as petrographic evidence of paragenetic complexity including compositional zoning and replacement textures among hydrothermal minerals. It would appear that overall rates of irreversible reactions between geothermal fluids and their mineralogic environment may, under certain circumstances, exceed transport rates governing energy and mass transfer so that local equilibrium conditions are temporally and spatially achieved in active geothermal environments.

As with the measured concentrations of aqueous silica, and alkali and alkaline Earth cations in geothermal fluids noted above, similar systematic relationships with respect to local solution-mineral equilibria have been reported between empirical and theoretical values for the concentration of CO_2. For example, a close correlation has been noted between CO_2 concentrations in geothermal fluids and values computed for equilibrium among alkali feldspars, epidote, layer-silicates (illite/muscovite) and

calcite for geothermal systems in silicic volcanic rocks (Taupo Volcanic Zone, New Zealand; Giggenbach, 1981) and in calcareous sediments (Salton Sea geothermal system, California; Bird and Norton, 1981). In basaltic rocks, Stefánsson and Arnórsson (2002) found that CO_2 concentrations estimated using reaction (1) are within an order of magnitude of measured CO_2 partial pressures in many Icelandic geothermal systems. Similar results have been obtained for aquifer fluids in geothermal fields at Krafla in Iceland (Gudmundsson and Arnórsson, 2002), Momtombo in Nicaragua (Arnórsson, 1996), Zunil in Guatemala (Arnórsson, 1995), Olkaria in Kenya (Karingithi and others, 2006) and Svartsengi in Iceland (Giroud unpublished work). In parts of the Olkaria and Krafla fields, however, calculated CO_2 partial pressures from geothermal fluids are considerably higher than those expected for solution-mineral equilibrium involving carbonate and calc-silicate mineral assemblages. This is attributed to unusually high CO_2 flux from magma heat sources, fluxes too high for attainment of local equilibrium with the common hydrothermal mineral parageneses (Gudmundsson and Arnórsson, 2002; Karingithi and others, 2006).

In the present study, we have built upon this previous body of research to evaluate the extent to which local equilibrium of epidote, prehnite, quartz, calcite and geothermal fluid provides a record of the concentration of CO_2. Our study illustrates that compositional variations in epidote (and prehnite; figs. 10 and 11) are a sensitive function of CO_2 concentrations and temperature (at pressures corresponding to liquid-vapor equilibrium of H_2O) required for local equilibrium of this assemblage. Any quantitative comparative analysis of P_{CO_2} derived from drill hole discharge fluids with values computed from equilibrium constraints imposed by reaction (1) must be viewed in terms of the nature of the samples analyzed. For the geothermal fluids, we note that discharge fluids are typically produced from a number of different input feed points within the drill hole, and thus sample different portions of the geothermal reservoir. Moreover, the uncertainty of P_{CO_2} in the geothermal reservoir fluid computed from chemical analyses of steam and liquid discharge is in itself dependent upon a combination of factors related to sampling, analytical and thermodynamic procedures. Likewise, mineralogic phase relations in this study are based on petrographic analysis of samples of the crushed lithology of drillhole cuttings that are typically < 2 mm in size, which precluded detailed analysis of paragenetic relationships among minerals and mineralized vein systems.

With these limitations in mind, we note that the fluids reported in table 1 are saturated with respect to quartz (fig. 12A), epidote (fig. 13B) and prehnite (fig. 13C). In terms of our adopted uncertainty of pH of $+/-0.3$, calcite is saturated, or at most slightly undersaturated with respect to the geothermal fluids over the temperature range of 275° to 310°C (fig. 13A), which represents the range of reference temperatures for our fluid analyses (tables 1 and 2). Within this temperature range, values of P_{CO_2} determined by chemical analysis of discharge fluids vary between ~1.3 to 4 bars (tables 1 and 2); this range decreases with increasing temperature (fig. 14A), but this may well be a sampling bias due to the larger number of lower-temperature samples analyzed. As a consequence, the shaded area in figure 14B corresponds to the overall range of P_{CO_2} reported in tables 1 and 2. The diamonds in figure 14B denote values of P_{CO_2} computed from individual epidote analyses (table A1) using equations and data presented above over the reference temperature range of 275° to 310°C. The solid diamonds (Assemblage) represent analyses of epidote crystals from drill cuttings from depth intervals where the epidote-prehnite-calcite-quartz assemblage has been reported (see figs. 3 and 7), whereas the open diamonds (Non-Assemblage) are analyses from drill cuttings where prehnite and/or calcite are not observed. Of the 143 epidote analyses from cuttings containing the assemblage epidote + prehnite + calcite + quartz (fig. 14B), 72 percent of the computed values of P_{CO_2} are within the range of

P_{CO_2} derived from analysis of collected formation fluids (1.3 to 4.0 bars; tables 1 and 2); this is graphically illustrated in the histogram of figure 15A. These computed "assemblage" values range from 0.57 to 6.17 bars. In contrast, of the 124 epidote analyses from drill cuttings that do not contain prehnite and/or calcite, 58 percent of the computed values of P_{CO_2} are within the range of derived P_{CO_2} values (see fig. 15B). These computed "non-assemblage" values range from 1.3 to 6.8 bars. If calcite is absent from the assemblage, the computation of P_{CO_2} using equilibria for reaction 1 provides the maximum value of P_{CO_2} at which calcite will not be present. Thus, our method for calculating fluid P_{CO_2} is proven quite reliable when all four index minerals of the epidote-prehnite-calcite-quartz assemblage are present. Additionally, if only epidote, prehnite and quartz are observed, our method appears to serve as a moderately accurate predictive proxy for fluid P_{CO_2} values in the Reykjanes geothermal system.

There are several explanations for the computed values of P_{CO_2} (diamonds in fig. 14B) that are greater than the measured values of the present day geothermal fluids represented by the shaded area in figure 14B. If calcite is not present in the assemblage (that is, the fluid is undersaturated with respect to calcite) then the computed value of P_{CO_2} (diamonds in fig. 14B) denotes a maximum value required for the absence of calcite. As the samples analyzed are drill cuttings, the presence of calcite in the cuttings does not necessarily require paragenetic equivalence with other mineral phases in the collective aggregate of the drill cuttings sample. We can see from figure 14B that epidotes denoted by the solid diamonds (Assemblage) that have values of $P_{CO_2} > 4$ bars are Al-rich epidotes ($X_{ps} < 0.25$) and at temperatures close to or exceeding 300°C. If calcite is not in equilibrium with epidote, prehnite and quartz in these samples then the high P_{CO_2} would represent a theoretical maximum value. However, if equilibrium for the assemblage is established then alternate explanations are required, such as local increases in P_{CO_2} due to magmatic intrusions (dikes). This alone highlights the importance of obtaining drill cores for evaluation of paragenetic relations of hydrothermal minerals in active geothermal systems.

Although complex chemical zoning is observed in epidotes from the Reykjanes geothermal system (fig. 5A), there is a general trend for the formation of Fe(III)-rich cores and Al-rich rims as illustrated in figures 5B and 6. If this zoning is formed while equilibrium is maintained among epidote + prehnite + calcite + quartz + fluid then the thermodynamic relationships illustrated in figures 11 and 14B provide possible explanations. For example, if the zoning for Fe(III)-rich core to Al-rich rim occurs under near isothermal conditions this would require an increase in P_{CO_2} with time. The rise in CO_2 content may likely record an increase in the number of high-level intrusions of dikes/sills and their magmatic degassing during the geologic evolution of this geothermal system. The most recent eruption on the Reykjanes peninsula was in 1226 C.E. and most of the peninsula is covered by 2000-year-old lava and also by subglacial hyaloclastites (fig. 2A; Saemundsson, 1997). Alternatively, if the zoning occurs under conditions of near constant P_{CO_2}, then equilibrium constraints imposed by reaction (1) requires that temperature decreases (see fig. 14B). The latter is likely in portions of the geothermal system as suggested by suppressed geotherms in well RN-17 relative to the high-temperature mineral zoning shown in figure 3.

Ultimately, the correlation between wellhead sampled and predicted fluid compositions provides insight into future abilities to characterize spatial and temporal concentrations of CO_2 in active and fossil hydrothermal and low-grade metamorphic environments in mafic lithologies based on compositional variations and paragenesis of hydrothermal minerals. In addition, this study will aid in our predictive understanding of the nature of reactions that involve natural sequestration of CO_2 derived from magmatic degassing, and injection of industrial CO_2-rich fluids within hydrothermal

environments in basaltic rocks. The latter is being field tested in the Hellisheidi area of Iceland (Oelkers and others, 2008).

ACKNOWLEDGMENTS

We appreciate constructive comments by Juhn Liou, Anne Egger, Emily Pope, Nellie Olsen, and Bob Jones (for analytical assistance). We wish to thank Axel Liebscher and Stuart Simmons for thoughtful, critical discussion that aided in the significant improvement of the manuscript. Research was funded by a Stanford University Vice Provost of Undergraduate Education Departmental Grant to AJEF, a Stanford University Undergraduate Research Programs quarter grant to AJEF, and by NSF EAR 0506882 to DKB.

Table A1

Summary of measured epidote composition data

Well	Depth	n_{Fe}	n_{Al}	X_{ps}	Well	Depth	n_{Fe}	n_{Al}	X_{ps}	Well	Depth	n_{Fe}	n_{Al}	X_{ps}	Well	Depth	n_{Fe}	n_{Al}	X_{ps}	Well	Depth	n_{Fe}	n_{Al}	X_{ps}
RN-10	1948	0.89	2.11	0.30	RN-10	1522	0.98	2.02	0.33	RN-10	1230	0.79	2.21	0.26	RN-10	1182	0.87	2.13	0.29	RN-10	1182	0.97	2.03	0.32
RN-10	1948	0.90	2.10	0.30	RN-10	1522	1.11	1.89	0.37	RN-10	1230	0.85	2.15	0.28	RN-10	1182	0.85	2.15	0.28	RN-10	1060	1.01	1.99	0.34
RN-10	1948	0.88	2.12	0.29	RN-10	1522	0.96	2.04	0.32	RN-10	1230	1.16	1.84	0.39	RN-10	1182	0.87	2.13	0.29	RN-10	1060	1.03	1.97	0.34
RN-10	1702	0.73	2.27	0.24	RN-10	1522	1.04	1.96	0.35	RN-10	1230	1.12	1.88	0.37	RN-10	1182	0.84	2.16	0.28	RN-10	1060	1.06	1.94	0.35
RN-10	1702	0.64	2.36	0.21	RN-10	1522	0.88	2.12	0.29	RN-10	1230	1.19	1.81	0.40	RN-10	1182	0.82	2.18	0.27	RN-10	1060	1.04	1.96	0.35
RN-10	1702	0.61	2.39	0.20	RN-10	1522	0.97	2.03	0.32	RN-10	1230	1.17	1.83	0.39	RN-10	1182	1.07	1.93	0.36	RN-10	1060	1.01	1.99	0.34
RN-10	1702	0.61	2.39	0.20	RN-10	1522	0.98	2.02	0.33	RN-10	1230	1.20	1.80	0.40	RN-10	1182	1.10	1.90	0.37	RN-10	1060	0.88	2.12	0.29
RN-10	1702	1.01	1.99	0.34	RN-10	1522	0.99	2.01	0.33	RN-10	1230	0.92	2.08	0.31	RN-10	1182	1.12	1.88	0.37	RN-10	1060	0.71	2.29	0.24
RN-10	1702	1.02	1.98	0.34	RN-10	1522	0.89	2.11	0.30	RN-10	1230	0.99	2.01	0.33	RN-10	1182	1.02	1.98	0.34	RN-10	1060	0.68	2.32	0.23
RN-10	1702	1.02	1.98	0.34	RN-10	1522	0.95	2.05	0.32	RN-10	1230	0.89	2.11	0.30	RN-10	1182	0.80	2.20	0.27	RN-10	1060	0.61	2.39	0.20
RN-10	1702	1.00	2.00	0.33	RN-10	1522	1.07	1.93	0.36	RN-10	1230	0.95	2.05	0.32	RN-10	1182	0.83	2.17	0.28	RN-10	1060	0.68	2.32	0.23
RN-10	1702	1.01	1.99	0.34	RN-10	1522	1.15	1.85	0.38	RN-10	1230	1.11	1.89	0.37	RN-10	1182	0.82	2.18	0.27	RN-10	1060	0.89	2.11	0.30
RN-10	1702	1.06	1.94	0.35	RN-10	1522	1.17	1.83	0.39	RN-10	1230	1.13	1.87	0.38	RN-10	1182	0.82	2.18	0.27	RN-10	1060	0.88	2.12	0.29
RN-10	1702	0.91	2.09	0.30	RN-10	1522	1.17	1.83	0.39	RN-10	1230	1.15	1.85	0.38	RN-10	1182	0.83	2.17	0.28	RN-10	1060	0.87	2.13	0.29
RN-10	1702	0.90	2.10	0.30	RN-10	1522	1.25	1.75	0.42	RN-10	1230	1.15	1.85	0.38	RN-10	1182	0.83	2.17	0.28	RN-10	1060	0.93	2.07	0.31
RN-10	1702	0.87	2.13	0.29	RN-10	1344	0.87	2.13	0.29	RN-10	1230	1.21	1.79	0.40	RN-10	1182	0.83	2.17	0.28	RN-10	1060	0.87	2.13	0.29
RN-10	1702	0.89	2.11	0.30	RN-10	1344	0.88	2.12	0.29	RN-10	1230	1.15	1.85	0.38	RN-10	1182	0.89	2.11	0.30	RN-10	1060	0.71	2.29	0.24
RN-10	1702	0.74	2.26	0.25	RN-10	1344	0.89	2.11	0.30	RN-10	1230	1.20	1.80	0.40	RN-10	1182	0.86	2.14	0.29	RN-10	1060	0.71	2.29	0.24
RN-10	1702	0.73	2.27	0.24	RN-10	1344	0.78	2.22	0.26	RN-10	1230	1.19	1.81	0.40	RN-10	1182	0.88	2.12	0.29	RN-10	1060	0.61	2.39	0.20
RN-10	1702	0.82	2.18	0.27	RN-10	1344	0.92	2.08	0.31	RN-10	1230	1.09	1.91	0.36	RN-10	1182	1.14	1.86	0.38	RN-10	1060	0.57	2.43	0.19
RN-10	1702	0.76	2.24	0.25	RN-10	1344	0.55	2.45	0.18	RN-10	1230	1.14	1.86	0.38	RN-10	1182	1.13	1.87	0.38	RN-10	1060	0.68	2.32	0.23
RN-10	1702	0.73	2.27	0.24	RN-10	1344	0.64	2.36	0.21	RN-10	1230	1.02	1.98	0.34	RN-10	1182	0.99	2.01	0.33	RN-10	1060	1.21	1.79	0.40
RN-10	1702	0.65	2.35	0.22	RN-10	1344	0.64	2.36	0.21	RN-10	1230	0.87	2.13	0.29	RN-10	1182	1.01	1.99	0.34	RN-10	1060	1.21	1.79	0.40
RN-10	1522	0.99	2.01	0.33	RN-10	1344	0.59	2.41	0.20	RN-10	1230	0.84	2.16	0.28	RN-10	1182	1.01	1.99	0.34	RN-10	1060	1.21	1.79	0.40
RN-10	1522	1.01	1.99	0.34	RN-10	1344	0.66	2.34	0.22	RN-10	1230	0.77	2.23	0.26	RN-10	1182	1.04	1.96	0.35	RN-10	1060	1.19	1.81	0.40
RN-10	1522	1.12	1.88	0.37	RN-10	1344	0.95	2.05	0.32	RN-10	1230	0.77	2.23	0.26	RN-10	1182	0.76	2.24	0.25	RN-10	1060	1.17	1.83	0.39
RN-10	1522	1.04	1.96	0.35	RN-10	1344	0.93	2.07	0.31	RN-10	1230	0.85	2.15	0.28	RN-10	1182	0.88	2.12	0.29	RN-10	1060	0.86	2.14	0.29
RN-10	1522	1.08	1.92	0.36	RN-10	1344	0.98	2.02	0.33	RN-10	1230	0.96	2.04	0.32	RN-10	1182	0.83	2.17	0.28	RN-10	1060	0.90	2.10	0.30
RN-10	1522	1.04	1.96	0.35	RN-10	1344	0.96	2.04	0.32	RN-10	1230	1.02	1.98	0.34	RN-10	1182	0.89	2.11	0.30	RN-10	1060	0.86	2.14	0.29
RN-10	1522	0.95	2.05	0.32	RN-10	1344	0.90	2.10	0.30	RN-10	1230	1.04	1.96	0.35	RN-10	1182	1.15	1.85	0.38	RN-10	1060	0.80	2.20	0.27
RN-10	1522	0.98	2.02	0.33	RN-10	1344	0.80	2.20	0.27	RN-10	1230	1.07	1.93	0.36	RN-10	1182	1.15	1.85	0.38	RN-10	1060	0.66	2.34	0.22
RN-10	1522	1.01	1.99	0.34	RN-10	1344	0.61	2.39	0.20	RN-10	1230	1.02	1.98	0.34	RN-10	1182	1.03	1.97	0.34	RN-10	1060	1.30	1.70	0.43
RN-10	1522	1.05	1.95	0.35	RN-10	1344	0.64	2.36	0.21	RN-10	1230	1.43	1.57	0.48	RN-10	1182	1.14	1.86	0.38	RN-10	1060	1.31	1.69	0.44
RN-10	1522	1.21	1.79	0.40	RN-10	1344	0.68	2.32	0.23	RN-10	1230	1.24	1.76	0.41	RN-10	1182	1.19	1.81	0.40	RN-10	1060	1.34	1.66	0.45
RN-10	1522	1.23	1.77	0.41	RN-10	1344	0.74	2.26	0.25	RN-10	1230	1.23	1.77	0.41	RN-10	1182	0.89	2.11	0.30	RN-10	1060	1.33	1.67	0.44
RN-10	1522	1.07	1.93	0.36	RN-10	1230	0.75	2.25	0.25	RN-10	1230	1.16	1.84	0.39	RN-10	1182	0.91	2.09	0.30	RN-10	1060	1.35	1.65	0.45
RN-10	1522	1.16	1.84	0.39	RN-10	1230	0.95	2.05	0.32	RN-10	1230	1.18	1.82	0.39	RN-10	1182	1.02	1.98	0.34	RN-10	1060	1.35	1.65	0.45
RN-10	1522	1.11	1.89	0.37	RN-10	1230	0.77	2.23	0.26	RN-10	1182	0.87	2.13	0.29	RN-10	1182	0.96	2.04	0.32	RN-10	1060	0.89	2.11	0.30

Table A1
(continued)

Well	Depth	n_{Fe}	n_{Al}	X_{ps}	Well	Depth	n_{Fe}	n_{Al}	X_{ps}	Well	Depth	n_{Fe}	n_{Al}	X_{ps}	Well	Depth	n_{Fe}	n_{Al}	X_{ps}	Well	Depth	n_{Fe}	n_{Al}	X_{ps}
RN-10	1060	0.86	2.14	0.29	RN-10	1430	0.86	2.14	0.29	RN-10	1148	1.11	1.89	0.37	RN-10	1430	1.04	1.96	0.35	RN-17	2600	0.78	2.22	0.26
RN-10	1060	0.97	2.03	0.32	RN-10	1430	0.71	2.29	0.24	RN-10	1148	1.05	1.95	0.35	RN-10	1430	1.15	1.85	0.38	RN-17	2600	0.84	2.16	0.28
RN-10	1060	0.88	2.12	0.29	RN-10	1430	0.73	2.27	0.24	RN-10	1148	0.75	2.25	0.25	RN-10	1430	1.14	1.86	0.38	RN-17	2600	0.85	2.15	0.28
RN-10	1872	1.06	1.94	0.35	RN-10	1430	0.78	2.22	0.26	RN-10	1148	0.67	2.33	0.22	RN-10	1430	1.15	1.85	0.38	RN-17	2600	0.83	2.17	0.28
RN-10	1872	1.06	1.94	0.35	RN-10	1430	1.03	1.97	0.34	RN-10	1148	0.67	2.33	0.22	RN-10	1430	0.87	2.13	0.29	RN-17	2600	0.86	2.14	0.29
RN-10	1872	1.02	1.98	0.34	RN-10	1430	1.02	1.98	0.34	RN-10	1148	0.69	2.31	0.23	RN-10	1430	0.89	2.11	0.30	RN-17	2600	0.69	2.31	0.23
RN-10	1872	1.03	1.97	0.34	RN-10	1430	1.03	1.97	0.34	RN-10	1148	0.91	2.09	0.30	RN-10	1430	0.89	2.11	0.30	RN-17	2600	0.86	2.14	0.29
RN-10	1872	1.03	1.97	0.34	RN-10	1430	1.04	1.96	0.35	RN-10	1148	0.91	2.09	0.30	RN-17	3050	0.63	2.37	0.21	RN-17	2600	0.83	2.17	0.28
RN-10	1872	0.90	2.10	0.30	RN-10	1430	1.02	1.98	0.34	RN-10	1148	0.95	2.05	0.32	RN-17	3050	0.76	2.24	0.25	RN-17	2600	0.90	2.10	0.30
RN-10	1872	0.79	2.21	0.26	RN-10	1430	1.03	1.97	0.34	RN-10	1148	0.92	2.08	0.31	RN-17	3050	0.80	2.20	0.27	RN-17	2600	0.51	2.49	0.17
RN-10	1872	0.81	2.19	0.27	RN-10	1430	1.02	1.98	0.34	RN-10	1148	0.92	2.08	0.31	RN-17	3050	0.82	2.18	0.27	RN-17	2600	0.63	2.37	0.21
RN-10	1872	0.81	2.19	0.27	RN-10	1430	0.99	2.01	0.33	RN-10	1148	0.96	2.04	0.32	RN-17	3050	0.69	2.31	0.23	RN-17	2600	0.80	2.20	0.27
RN-10	1872	0.78	2.22	0.26	RN-10	1430	0.75	2.25	0.25	RN-10	1148	0.88	2.12	0.29	RN-17	3050	0.72	2.28	0.24	RN-17	2600	0.79	2.21	0.26
RN-10	1872	1.10	1.90	0.37	RN-10	1430	0.78	2.22	0.26	RN-10	1148	0.67	2.33	0.22	RN-17	3050	0.77	2.23	0.26	RN-17	2600	0.74	2.26	0.25
RN-10	1872	1.14	1.86	0.38	RN-10	1430	1.00	2.00	0.33	RN-10	1148	0.62	2.38	0.21	RN-17	3050	0.77	2.23	0.26	RN-17	2600	0.71	2.29	0.24
RN-10	1872	1.10	1.90	0.37	RN-10	1430	1.00	2.00	0.33	RN-10	1148	0.97	2.03	0.32	RN-17	3050	0.85	2.15	0.28	RN-17	2600	0.87	2.13	0.29
RN-10	1872	1.08	1.92	0.36	RN-10	1430	1.01	1.99	0.34	RN-10	1148	0.96	2.04	0.32	RN-17	3050	0.84	2.16	0.28	RN-17	1650	0.99	2.01	0.33
RN-10	1872	1.06	1.94	0.35	RN-10	1430	1.01	1.99	0.34	RN-10	1148	0.97	2.03	0.32	RN-17	3050	0.86	2.14	0.29	RN-17	1650	1.06	1.94	0.35
RN-10	1872	1.06	1.94	0.35	RN-10	1430	1.00	2.00	0.33	RN-10	1148	0.97	2.03	0.32	RN-17	3050	0.77	2.23	0.26	RN-17	1650	1.09	1.91	0.36
RN-10	1872	1.05	1.95	0.35	RN-10	1430	1.00	2.00	0.33	RN-10	1148	0.98	2.02	0.33	RN-17	3050	0.84	2.16	0.28	RN-17	1650	0.95	2.05	0.32
RN-10	1872	0.82	2.18	0.27	RN-10	1430	0.99	2.01	0.33	RN-10	1148	0.98	2.02	0.33	RN-17	3050	0.80	2.20	0.27	RN-17	1650	0.92	2.08	0.31
RN-10	1872	0.81	2.19	0.27	RN-10	1430	0.86	2.14	0.29	RN-10	1148	1.01	1.99	0.34	RN-17	3050	0.71	2.29	0.24	RN-17	1650	0.96	2.04	0.32
RN-10	1872	0.70	2.30	0.23	RN-10	1430	0.82	2.18	0.27	RN-10	1148	0.71	2.29	0.24	RN-17	2150	0.75	2.25	0.25	RN-17	1650	0.96	2.04	0.32
RN-10	1430	0.91	2.09	0.30	RN-10	1430	0.76	2.24	0.25	RN-10	1148	0.66	2.34	0.22	RN-17	2150	0.80	2.20	0.27	RN-17	1650	1.12	1.88	0.37
RN-10	1430	0.90	2.10	0.30	RN-10	1148	0.95	2.05	0.32	RN-10	1148	0.65	2.35	0.22	RN-17	2150	0.72	2.28	0.24	RN-17	1650	1.22	1.78	0.41
RN-10	1430	0.87	2.13	0.29	RN-10	1148	0.98	2.02	0.33	RN-10	1148	1.02	1.98	0.34	RN-17	2150	0.55	2.45	0.18	RN-17	1650	1.00	2.00	0.33
RN-10	1430	0.88	2.12	0.29	RN-10	1148	0.96	2.04	0.32	RN-10	1148	1.03	1.97	0.34	RN-17	2150	0.70	2.30	0.23	RN-17	1650	0.81	2.19	0.27
RN-10	1430	0.90	2.10	0.30	RN-10	1148	0.80	2.20	0.27	RN-10	1148	1.02	1.98	0.34	RN-17	2150	0.80	2.20	0.27	RN-17	1650	0.86	2.14	0.29
RN-10	1430	1.16	1.84	0.39	RN-10	1148	0.69	2.31	0.23	RN-10	1148	1.03	1.97	0.34	RN-17	2150	0.78	2.22	0.26	RN-17	1650	0.91	2.09	0.30
RN-10	1430	1.19	1.81	0.40	RN-10	1148	0.81	2.19	0.27	RN-10	1148	1.06	1.94	0.35	RN-17	2150	0.65	2.35	0.22	RN-17	1800	0.88	2.12	0.29
RN-10	1430	1.21	1.79	0.40	RN-10	1148	0.82	2.18	0.27	RN-10	1148	1.04	1.96	0.35	RN-17	2150	0.66	2.34	0.22	RN-17	1800	0.67	2.33	0.22
RN-10	1430	1.24	1.76	0.41	RN-10	1148	0.71	2.29	0.24	RN-10	1148	1.01	1.99	0.34	RN-17	2150	0.81	2.19	0.27	RN-17	1800	0.80	2.20	0.27
RN-10	1430	0.95	2.05	0.32	RN-10	1148	0.68	2.32	0.23	RN-10	1148	0.70	2.30	0.23	RN-17	2150	0.76	2.24	0.25	RN-17	1800	0.74	2.26	0.25
RN-10	1430	0.94	2.06	0.31	RN-10	1148	0.60	2.40	0.20	RN-10	1148	0.67	2.33	0.22	RN-17	2150	0.81	2.19	0.27	RN-17	1800	0.71	2.29	0.24
RN-10	1430	0.90	2.10	0.30	RN-10	1148	1.08	1.92	0.36	RN-10	1148	0.62	2.38	0.21	RN-17	2150	0.69	2.31	0.23	RN-17	1800	0.93	2.07	0.31
RN-10	1430	0.91	2.09	0.30	RN-10	1148	1.06	1.94	0.35	RN-10	1430	1.07	1.93	0.36	RN-17	2150	0.77	2.23	0.26	RN-17	1800	0.92	2.08	0.31
RN-10	1430	0.94	2.06	0.31	RN-10	1148	1.06	1.94	0.35	RN-10	1430	1.08	1.92	0.36	RN-17	2150	0.89	2.11	0.30	RN-17	1800	0.87	2.13	0.29
RN-10	1430	0.91	2.09	0.30	RN-10	1148	1.14	1.86	0.38	RN-10	1430	1.03	1.97	0.34	RN-17	2150	0.71	2.29	0.24	RN-17	1800	0.73	2.27	0.24

Table A1

(continued)

Well	Depth	n_{Fe}	n_{Al}	X_{ps}	Well	Depth	n_{Fe}	n_{Al}	X_{ps}	Well	Depth	n_{Fe}	n_{Al}	X_{ps}	Well	Depth	n_{Fe}	n_{Al}	X_{ps}	Well	Depth	n_{Fe}	n_{Al}	X_{ps}
RN-17	1800	0.69	2.31	0.23	RN-17	1150	1.03	1.97	0.34	RN-17	800	1.02	1.98	0.34	RN-17	700	1.03	1.97	0.34	RN-17	2500	0.85	2.15	0.28
RN-17	1800	0.70	2.30	0.23	RN-17	1150	0.71	2.29	0.24	RN-17	800	0.95	2.05	0.32	RN-17	700	1.07	1.93	0.36	RN-17	2500	0.86	2.14	0.29
RN-17	1800	0.77	2.23	0.26	RN-17	1150	0.74	2.26	0.25	RN-17	800	1.00	2.00	0.33	RN-17	700	1.00	2.00	0.33	RN-17	2500	0.83	2.17	0.28
RN-17	1800	0.83	2.17	0.28	RN-17	1150	0.71	2.29	0.24	RN-17	800	0.93	2.07	0.31	RN-17	500	1.02	1.98	0.34	RN-17	2500	0.65	2.35	0.22
RN-17	1800	0.79	2.21	0.26	RN-17	1150	1.03	1.97	0.34	RN-17	800	0.95	2.05	0.32	RN-17	500	1.02	1.98	0.34	RN-17	2500	0.75	2.25	0.25
RN-17	1800	0.76	2.24	0.25	RN-17	1150	1.03	1.97	0.34	RN-17	600	0.71	2.29	0.24	RN-17	500	0.96	2.04	0.32	RN-17	2500	0.73	2.27	0.24
RN-17	1800	0.78	2.22	0.26	RN-17	1150	1.05	1.95	0.35	RN-17	600	0.71	2.29	0.24	RN-17	500	1.03	1.97	0.34	RN-17	2500	0.69	2.31	0.23
RN-17	1800	0.71	2.29	0.24	RN-17	1150	1.00	2.00	0.33	RN-17	600	0.95	2.05	0.32	RN-17	500	0.95	2.05	0.32	RN-17	2500	0.71	2.29	0.24
RN-17	1800	0.73	2.27	0.24	RN-17	1150	0.62	2.38	0.21	RN-17	600	0.73	2.27	0.24	RN-17	500	0.97	2.03	0.32	RN-17	2500	0.74	2.26	0.25
RN-17	1800	0.69	2.31	0.23	RN-17	1150	0.75	2.25	0.25	RN-17	600	0.82	2.18	0.27	RN-17	500	1.00	2.00	0.33	RN-17	2500	0.59	2.41	0.20
RN-17	1400	0.79	2.21	0.26	RN-17	1150	1.08	1.92	0.36	RN-17	600	0.80	2.20	0.27	RN-17	500	1.01	1.99	0.34	RN-17	2500	0.60	2.40	0.20
RN-17	1400	0.79	2.21	0.26	RN-17	1000	0.96	2.04	0.32	RN-17	600	0.92	2.08	0.31	RN-17	500	0.97	2.03	0.32	RN-17	2500	0.71	2.29	0.24
RN-17	1400	0.78	2.22	0.26	RN-17	1000	0.96	2.04	0.32	RN-17	600	1.06	1.94	0.35	RN-17	500	1.09	1.91	0.36	RN-17	2500	0.87	2.13	0.29
RN-17	1400	0.67	2.33	0.22	RN-17	1000	0.97	2.03	0.32	RN-17	600	1.09	1.91	0.36	RN-17	500	1.05	1.95	0.35	RN-17	2500	0.85	2.15	0.28
RN-17	1400	0.65	2.35	0.22	RN-17	1000	0.90	2.10	0.30	RN-17	600	0.91	2.09	0.30	RN-17	500	0.99	2.01	0.33	RN-17	2500	0.86	2.14	0.29
RN-17	1400	0.74	2.26	0.25	RN-17	1000	0.82	2.18	0.27	RN-17	600	0.96	2.04	0.32	RN-17	500	1.03	1.97	0.34	RN-17	2900	1.05	1.95	0.35
RN-17	1400	0.78	2.22	0.26	RN-17	1000	0.77	2.23	0.26	RN-17	600	0.92	2.08	0.31	RN-17	500	1.15	1.85	0.38	RN-17	2900	1.06	1.94	0.35
RN-17	1400	0.78	2.22	0.26	RN-17	1000	0.81	2.19	0.27	RN-17	600	0.82	2.18	0.27	RN-17	500	1.03	1.97	0.34	RN-17	2900	1.06	1.94	0.35
RN-17	1400	0.76	2.24	0.25	RN-17	1000	0.64	2.36	0.21	RN-17	600	0.80	2.20	0.27	RN-17	500	1.03	1.97	0.34	RN-17	2900	1.06	1.94	0.35
RN-17	1400	0.84	2.16	0.28	RN-17	1000	0.84	2.16	0.28	RN-17	600	0.80	2.20	0.27	RN-17	500	1.04	1.96	0.35	RN-17	2900	1.06	1.94	0.35
RN-17	1400	0.79	2.21	0.26	RN-17	1000	0.83	2.17	0.28	RN-17	600	0.86	2.14	0.29	RN-17	500	1.07	1.93	0.36	RN-17	2900	1.06	1.94	0.35
RN-17	1400	0.73	2.27	0.24	RN-17	1000	1.35	1.65	0.45	RN-17	600	0.91	2.09	0.30	RN-17	500	0.99	2.01	0.33	RN-17	2900	0.74	2.26	0.25
RN-17	1400	0.69	2.31	0.23	RN-17	1000	1.34	1.66	0.45	RN-17	600	1.04	1.96	0.35	RN-17	500	0.97	2.03	0.32	RN-17	2900	0.74	2.26	0.25
RN-17	1400	0.87	2.13	0.29	RN-17	1000	1.19	1.81	0.40	RN-17	600	0.89	2.11	0.30	RN-17	2800	0.92	2.08	0.31	RN-17	2900	0.70	2.30	0.23
RN-17	1400	0.78	2.22	0.26	RN-17	1000	1.17	1.83	0.39	RN-17	600	0.99	2.01	0.33	RN-17	2800	0.91	2.09	0.30	RN-17	2900	0.84	2.16	0.28
RN-17	1150	1.13	1.87	0.38	RN-17	1000	1.25	1.75	0.42	RN-17	600	0.90	2.10	0.30	RN-17	2800	0.90	2.10	0.30	RN-17	2900	1.06	1.94	0.35
RN-17	1150	1.12	1.88	0.37	RN-17	1000	1.20	1.80	0.40	RN-17	600	0.88	2.12	0.29	RN-17	2800	0.94	2.06	0.31	RN-17	2900	1.07	1.93	0.36
RN-17	1150	1.03	1.97	0.34	RN-17	1000	1.16	1.84	0.39	RN-17	600	0.85	2.15	0.28	RN-17	2800	0.95	2.05	0.32	RN-17	2900	0.99	2.01	0.33
RN-17	1150	1.03	1.97	0.34	RN-17	1000	1.15	1.85	0.38	RN-17	600	0.81	2.19	0.27	RN-17	2800	0.74	2.26	0.25	RN-17	2900	0.97	2.03	0.32
RN-17	1150	0.99	2.01	0.33	RN-17	1000	1.23	1.77	0.41	RN-17	700	0.99	2.01	0.33	RN-17	2800	0.73	2.27	0.24	RN-17	2900	0.96	2.04	0.32
RN-17	1150	1.04	1.96	0.35	RN-17	1000	1.38	1.62	0.46	RN-17	700	0.73	2.27	0.24	RN-17	2800	0.82	2.18	0.27	RN-17	2900	0.72	2.28	0.24
RN-17	1150	1.02	1.98	0.34	RN-17	800	0.93	2.07	0.31	RN-17	700	0.71	2.29	0.24	RN-17	2800	0.71	2.29	0.24	RN-17	2900	0.65	2.35	0.22
RN-17	1150	1.03	1.97	0.34	RN-17	800	0.86	2.14	0.29	RN-17	700	0.91	2.09	0.30	RN-17	2800	0.72	2.28	0.24	RN-17	2900	0.82	2.18	0.27
RN-17	1150	1.02	1.98	0.34	RN-17	800	0.98	2.02	0.33	RN-17	700	0.89	2.11	0.30	RN-17	2500	0.84	2.16	0.28					

Columns of n_{Fe} and n_{Al} display the total Fe(III) and Al detected in epidote analyses, which have been normalized to three octahedral sites. Dark gray rows indicate "assemblage" values, or depths at which the reference temperature is between 275 and 310°C and all members of the epidote-prehnite-calcite-quartz assemblage are observed. Light gray rows indicate "non-assemblage" values, or depths at which the reference temperature is between 275 and 310°C, but not all members of the assemblage are observed. White rows indicate either depths at which the reference temperature is below 275°C or above 310°C, or if $X_{ps} > 0.36$ [contains more Fe(III) than the most Fe(III)-rich epidotes that are observed in cuttings from the same depth as prehnite]. Epidote compositions from all rows are displayed in figure 7 as a function of depth.

TABLE A2

Representative epidote chemical analyses

Well	**RN-9**	**RN -17**	**RN-17**	**RN-10**	**RN-10**
Depth	846	2500	2800	1148	1430
SiO_2	36.81	38.02	37.12	35.84	36.96
Al_2O_3	20.47	26.06	22.08	19.71	21.84
TiO_2	-	0.10	0.12	0.62	0.03
Cr_2O_3	-	0.00	0.01	0.02	0.04
Fe_2O_3	16.15	10.16	14.70	16.19	14.50
MnO	-	0.11	0.01	0.06	0.08
MgO	-	0.04	0.09	0.13	0.06
CaO	22.13	22.76	22.92	22.06	22.61
Na_2O	-	0.02	0.00	0.00	0.01
K_2O	-	0.00	0.01	0.00	0.00
Total	95.75	97.27	97.07	94.64	96.13
	Formula based on 8 cations				
Si	3.0263	3.0028	2.9981	2.9935	3.0125
Al	1.9832	2.4252	2.1018	1.9408	2.0978
Ti	-	0.0061	0.0076	0.0390	0.0016
Cr	-	0.0000	0.0006	0.0012	0.0023
Fe^{3+}	0.9990	0.6037	0.8936	1.0176	0.8891
∑(VI)	2.9822	3.0349	3.0036	2.9986	2.9908
Mn	-	0.0071	0.0009	0.0043	0.0057
Mg	-	0.0050	0.0106	0.0168	0.0067
Ca	1.9491	1.9255	1.9828	1.9745	1.9747
Na	-	0.0028	0.0000	0.0000	0.0016
K	-	0.0000	0.0008	0.0000	0.0000
∑(VII)	1.9491	1.9404	1.9951	1.9955	1.9888

TABLE A3

Summary of measured prehnite composition data

Well	Depth	n_{Si}	n_{Al}	$n_{Al\text{-}Oct*}$	n_{Fe}	n_{Ca}	Formula Total
RN-17	700	3.03	1.66	0.70	0.32	1.88	17.98
RN-17	700	3.00	1.67	0.67	0.33	1.95	17.99
RN-17	700	3.02	1.62	0.64	0.32	1.98	18.00
RN-17	700	3.01	1.59	0.59	0.42	1.95	17.99
RN-17	700	3.01	1.62	0.63	0.38	1.95	17.99
RN-17	700	3.01	1.66	0.67	0.34	1.97	17.99
RN-17	700	3.05	1.63	0.68	0.32	1.97	17.98
RN-17	700	2.98	1.86	0.85	0.15	1.98	18.00
RN-17	700	2.97	1.48	0.45	0.55	1.99	18.01
RN-17	800	3.00	1.57	0.57	0.44	1.96	17.99
RN-17	800	3.02	1.70	0.72	0.29	1.95	17.98
RN-17	800	3.02	1.74	0.76	0.27	1.93	17.98
RN-17	800	3.04	1.60	0.64	0.38	1.92	17.96
RN-17	800	3.03	1.64	0.67	0.31	1.98	17.99
RN-17	800	3.00	1.71	0.70	0.34	1.92	17.98
RN-17	800	3.05	1.79	0.84	0.18	1.94	17.97
RN-17	800	3.03	1.72	0.75	0.28	1.91	17.97
RN-17	800	3.04	1.69	0.73	0.27	1.95	17.97
RN-17	800	3.03	1.86	0.89	0.13	1.94	17.97
RN-17	800	3.04	1.85	0.89	0.14	1.92	17.96
RN-17	800	3.07	1.69	0.76	0.26	1.91	17.94
RN-17	800	3.00	1.41	0.41	0.59	1.99	18.00
RN-17	800	3.03	1.55	0.59	0.42	1.96	17.98
RN-17	800	3.02	1.68	0.70	0.31	1.96	17.98
RN-17	800	2.99	1.62	0.62	0.37	2.00	18.00
RN-17	800	3.01	1.54	0.55	0.46	1.96	17.99
RN-17	800	3.01	1.63	0.64	0.37	1.99	17.99
RN-17	800	3.03	1.44	0.47	0.54	1.97	17.98
	Average:	3.02	1.65	0.67	0.34	1.95	17.98

* Since Al and Si commonly share four tetrahedral sites in prehnite in a 3 Si:1 Al ratio (with some degree of substitution for one another), the number of Al atoms in the octahedral sites $= 4 - n_{Si}$. Therefore, the computed $X_{Al,Octahedral} = n_{Al} - (4 - n_{Si})$.

REFERENCES

Akaku, K., Reed, M. H., Yagi, M., Kai, K., and Yasuda, Y., 1991, Chemical and physical processes occurring in the Fushime geothermal system, Kyushu, Japan: Geochemical Journal, v. 25, p. 315–333.

Ármannsson, H., Gíslason, G., and Hauksson, T., 1982, Magmatic gases in well fluids aid the mapping of flow pattern in a geothermal system: Geochimica et Cosmochimica Acta, v. 46, p. 167–177, doi:10.1016/0016-7037(82)90244-7.

Arnason, J. G., and Bird, D. K., 1992, Formation of zoned epidote in hydrothermal Systems: International Symposium on Water-Rock Interaction, v. 7, p. 1,473–1,476.

Arnason, J. G., Bird, D. K., and Liou, J. G., 1993, Variables controlling epidote composition in hydrothermal and low-pressure regional metamorphic rocks: Abhandlungen der Geologischen Bundesantalt, v. 49, p. 17–25.

Arnórsson, S., 1970, Underground temperatures in hydrothermal areas in Iceland as deduced from the silica content of the thermal water: Geothermics, v. 2, p. 536–541, doi:10.1016/0375-6505(70)90052-0.

——— 1975, Application of the silica geothermometer in low temperature hydrothermal areas in Iceland: American Journal of Science, v. 275, p. 763–784.
——— 1978, Major element chemistry of the geothermal sea-water at Reykjanes and Svartsengi, Iceland: Mineralogical Magazine, v. 42, p. 209–220, doi:10.1180/minmag.1978.042.322.07.
——— 1985, The use of mixing models and chemical geothermometers for estimating underground temperatures in geothermal systems: Journal of Volcanology and Geothermal Research, v. 23, p. 209–335, doi:10.1016/0377-0273(85)90039-3.
——— 1995, Geothermal systems in Iceland; structure and conceptual models; I, High-temperature areas: Geothermics, v. 24, p. 561–602, doi:10.1016/0375-6505(95)00025-9.
——— 1996, Interpretation of chemical and isotopic data on fluids discharges from wells in the Momotombo geothermal field, Nicaragua: International Atomic Energy Agency, report NIC/8/008-04, 21 p.
Arnórsson, S., and Gunnlaugsson, E., 1985, New gas geothermometers for geothermal exploration-calibration and application: Geochimica et Cosmochimica Acta, v. 49, p. 1,307–1,325, doi:10.1016/0016-7037(85)90283-2.
Arnórsson, S., Grönvold, K., and Sigurdsson, S., 1978, Aquifer chemistry of four high-temperature geothermal systems in Iceland: Geochimica et Cosmochimica Acta, v. 42, p. 523–536, doi:10.1016/0016-7037(78)90202-8.
Arnórsson, S., Sigurdsson, S., and Svavarsson, H., 1982, The chemistry of geothermal waters in Iceland. I, Calculation of aqueous speciation from 0° to 370° C: Geochimica et Cosmochimica Acta, v. 46, p. 1,513–1,532, doi:10.1016/0016-7037(82)90311-8.
Arnórsson, S., Gunnlaugsson, E., and Svavarsson, H., 1983, The chemistry of geothermal waters in Iceland. III. Chemical geothermometry in geothermal investigations: Geochimica et Cosmochimica Acta, v. 47, p. 567–577, doi:10.1016/0016-7037(83)90278-8.
Arnórsson S., Gunnarsson, I., Stefánsson, A., Andresdottir, A., and Sveinbjörnsdóttir, A. E., 2002, Major element chemistry of surface and ground waters in basaltic terrain, N-Iceland. I. Primary mineral saturation: Geochimica et Cosmochimica Acta, v. 66, p. 4,015–4,046, doi:10.1016/S0016-7037(02)00991-2.
Arnórsson, S., Stefánsson, A, and Bjarnason, J. O., 2007, Fluid-Fluid Interactions in Geothermal Systems: Reviews in Mineralogy and Geochemistry, v. 65, p. 259–312, doi:10.2138/rmg.2007.65.9.
Bird, D. K., and Helgeson, H. C., 1980, Chemical interaction of aqueous solutions with epidote-feldspar mineral assemblages in geologic systems. I. Thermodynamic analysis of phase relations in the system CaO-FeO-Fe_2O_3-Al_2O_3-SiO_2-H_2O-CO_2: American Journal of Science, v. 280, p. 907–941.
——— 1981, Chemical interaction of aqueous solutions with epidote-feldspar mineral assemblages in geologic systems. II. Equilibrium constraints in metamorphic/geothermal processes: American Journal of Science, v. 281, p. 576–614.
Bird, D. K., and Norton, D. L., 1981, Theoretical prediction of phase relations among aqueous solutions and minerals: Salton Sea geothermal system: Geochimica et Cosmochimica Acta, v. 45, p. 1,479–1,493, doi:10.1016/0016-7037(81)90280-5.
Bird, D. K., and Spieler, A. R., 2004, Epidote in geothermal systems: Reviews in Mineralogy and Geochemistry, v. 56, p. 235–300, doi: 10.2138/gsrmg.56.1.235.
Bird, D. K., Schiffman, P., Elders, W. A., Williams, A. E., and McDowell, S. D., 1984, Calc-silicate mineralization in active geothermal systems: Economic Geology, v. 79, p. 671–695.
Bird, D. K., Cho, M., Janik, C. J., Liou, J. G., and Caruso, L. J., 1988, Compositional, order/disorder, and stable isotope characteristics of Al-Fe epidote, State 2-14 drill hole, Salton Sea geothermal system: Journal of Geophysical Research: Solid Earth, v. 93(B11), p. 13,135–13,144.
Bjarnason, J. O., 1994, The speciation program WATCH version 2.1A: Icelandic National Energy Authority Report, 7 p.
Björnsson, S., Arnórsson, S., and Tómasson, J., 1972, Economic evaluation of the Reykjanes thermal brine area, Iceland: American Association of Petroleum Geologists Bulletin, v. 56, p. 2,380–2,391.
Bredehoeft, J. D., and Norton, D. L., editors, 1990, The role of fluids in crustal processes: Washington D. C., National Academy Press, 170 p.
Cathles, L. M., 1977, An analysis of the cooling of intrusives by groundwater convection which includes boiling: Economic Geology, v. 72, p. 804–826, doi:10.2113/gsecongeo.72.5.804.
Cathles, L. M., Erendi, A. H. J., Theyer, J. B., and Barrie, C. T., 1997, How long can a hydrothermal system be sustained by a single intrusion event?: Economic Geology, v. 92, p. 766–771, doi:10.2113/gsecongeo.92.7-8.766.
Conrad, C. P., Lithgow-Bertelloni, C., and Louden, K. E., 2004, Iceland, the Farallon Slab, and the Dynamic Topography of the North Atlantic: Geology, v. 32, p. 177–180, doi:10.1130/G20137.1.
Deer, W. A., Howie, R. A., and Zussman, J., 1962, Rock-forming minerals, v. 1, Ortho and Ring Silicates: New York, John Wiley and Sons, Inc., 333 p.
Dollase, W. A., 1971, Refinement of the crystal structures of epidote, allanite and hancockite: American Mineralogist, v. 56, p. 447–464.
——— 1973, Mössbauer spectra and iron distribution in the epidote group minerals: Zeitschrift fuer Kristallographie, v. 138, p. 41–63.
Fehr, K. T., and Heuss-Aßhichler, S., 1997, Intracrystalline equilibria and immiscibility along the join clinozoisite-epidote: an experimental and ^{57F}e-Mössbauer study: Neues Jahrbuch Fur Mineralogie-Abhandlungen, v. 172, p. 43–67.
Fernandez-Prini, R., Alvarez, J. L., and Harvey, A. H., 2003, Henry's constants and vapor-liquid distribution constants for gaseous solutes in H_2O and D_2O at high temperatures: Journal of Physical Chemistry Ref. Data, v. 32, p. 903–916.

Fournier, R. O., 1973, Silica in thermal waters: laboratory and field investigations, *in* Proceedings International Symposium on Hydrogeology and Biogeochemistry, Tokyo, 1970: Hydrogeochemistry, v. 1, p. 122–139.
——— 1977, Chemical geothermometers and mixing models for geothermal Systems: Geothermics, v. 5, p. 41–50, doi:10.1016/0375-6505(77)90007-4.
——— 1983, A method of calculating quartz solubilities in aqueous sodium chloride solutions: Geochimica et Cosmochimica Acta, v. 47, p. 579–586, doi:10.1016/0016-7037(83)90279-X.
Fournier, R. O., and Potter, R. W., II, 1979. Magnesium correction to the Na-K-Ca chemical geothermometer: Geochimica et Cosmochimica Acta, v. 43, p. 1,543–1,550, doi:10.1016/0016-7037(79)90147-9.
——— 1982, A revised and expanded silica (quartz) Geothermometer: Geothermal Resources Council Bulletin, v. 11, p. 3–12.
Fournier, R. O., and Rowe, J. J., 1977, The solubility of amorphous silica in water at high temperatures and pressures: American Mineralogist, v. 62, p. 1,052–1,056.
Fournier, R. O., and Truesdell, A. H., 1973, An empirical Na-K-Ca geothermometer for natural waters: Geochimica Cosmochimica Acta, v. 37, p. 1,255–1,275, doi:10.1016/0016-7037(73)90060-4.
Franz, G., and Liebscher, A., 2004, Epidotes: Reviews in Mineralogy and Geochemistry, v. 56, 638 p.
Franzson, H., 1990, Svartsengi. Geological model of a high temperature system and its surroundings: Orkustofnun Report OS-90050/JHD-08, 41 p., (in Icelandic with English summary).
——— 2000, Reykjanes. Rannsóknir á vökvabólum í útfellingum í holum RN-9 og RN-10: Orkustofnun Report, OS-2000/021, 20 p., (in Icelandic).
Franzson, H., Thordarson, S., Björnsson, G., Gudlaugsson, S. T., Richter, B., Fridleifsson, G. O., and Thorhallsson, S., 2002, Reykjanes high-temperature field, SW-Iceland. Geology and hydrothermal alteration of well RN-10: Stanford, California, Stanford University, Workshop on Geothermal Reservoir Engineering 27, p. 233–240.
Fridleifsson, G. Ó., and Albertsson, A., 2000, Deep geothermal drilling on the Reykjanes Ridge: Opportunity for international collaboration: Proceedings of the World Geothermal Congress 2000, International Geothermal Organization, Paper R0882, p. F7-5.
Fridleifsson, G. O., and Elders, W. A., 2005, The Iceland Deep Drilling Project: A search for deep unconventional geothermal resources: Geothermics, v. 34, p. 269–285, doi:10.1016/j.geothermics.2004.11.004.
Fridleifsson, G. O., Blischke, A., Kristjánsson, B. R., Richter, B., Einarsson, G. M., Jónasson, H., Franzson, H., Sigurdsson, O., Danielsen, P. E., Jónsson, S. S., Thordarson, S., Thórhallsson, S., Hardardóttir, V., and Egilson, Th., 2005, Reykjanes Well Report RN-17 & RN-17ST: Iceland Geosurvey Report ISOR-2005/007.
Fridriksson, Th., and Giroud, N., 2008, Geochemical production monitoring at Reykjanes 2006 and 2007: Iceland GeoSurvey Report ISOR-2008/021, 53 p., (in Icelandic).
Giggenbach, W. F., 1981, Geothermal mineral equilibria: Geochimica et Cosmochimica Acta, v. 45, p. 393–410, doi:10.1016/0016-7037(81)90248-9.
Giggenbach, W. F., and Stewart, M. K., 1982, Processes controlling the isotopic composition of steam and water discharges from steam vents and steam-heated pools in geothermal areas: Geothermics, v. 11, p. 71–80, doi:10.1016/0375-6505(82)90009-8.
Giuli, G., Bonazzi, P., and Menchetti, S., 1999, Al-Fe disorder in synthetic epidotes: A single-crystal x-ray diffraction study: American Mineralogist, v. 84, p. 933–936.
Gottschalk, M., 2004, Thermodynamic properties of zoisite, clinozoisite, and epidote, *in* Liebscher, A., and Franz, B., editors, Epidotes: Reviews in Mineralogy and Geochemistry, v. 56, p. 83–124, doi: 10.2138/gsrmg.56.1.83.
Grapes, R. H., and Hoskin, P. W. O., 2004, Epidote group minerals in low-medium pressure metamorphic terrains, *in* Liebscher, A., and Franz, B., editors, Epidotes: Reviews in Mineralogy and Geochemistry, v. 56, p. 301–345, doi:10.2138/gsrmg.56.1.301.
Gudmundsson, Á., 1986, Mechanical aspects of postglacial volcanism and tectonics of the Reykjanes Peninsula, Southwest Iceland: Journal of Geophysical Research, v. 91(B12), p. 12,711–12,721, doi: 10.1029/JB091iB12p12711.
——— 1987, Formation and mechanics of magma reservoirs in Iceland: Geophysical Journal of the Royal Astronomical Society, v. 91, p. 27–41, doi: 10.1111/j.1365-246X.1987.tb05211.x.
Gudmundsson, B. T., and Arnórsson, S., 2002, Geochemical monitoring of the Krafla and Namafjall geothermal areas, N-Iceland: Geothermics, v. 31, p. 195–243, doi:10.1016/S0375-6505(01)00022-0.
Hardardóttir, V., Ármannsson, H., and Thorhallsson, S., 2005, Characterization of sulfide-Rich Scales in Brine at Reykjanes: Antalya, Turkey, Proceedings World Geothermal Congress 2005, p. 1–8.
Hashimoto, M., 1964, The chemistry and optics of prehnite: The Journal of the Geological Society of Japan, v. 70, p. 180–183.
Helgeson, H. C., 1981, Prediction of the thermodynamic properties of electrolytes at high temperatures and pressures, *in* Wickman, F. E., and Rickard, D. T., editors, Chemistry and geochemistry of solutions at high temperatures and pressures: Proceedings of a Nobel Symposium: Stockholm, Royal Swedish Academy of Sciences.
Helgeson, H. C., Delany, J. M., Nesbitt, H. W., and Bird, D. K., 1978, Summary and critique of the thermodynamic properties of rock-forming minerals: American Journal of Science, v. 278A, p. 1–229.
Henley, R. W., and Ellis, A. J., 1983, Geothermal Systems Ancient and Modern: A Geochemical Review: Earth-Science Reviews, v. 19, p. 1–50, doi:10.1016/0012-8252(83)90075-2.
Hjartarson, A., 2006, Reiknilíkan af jardhitakerfinu á Reykjanesi og spár um vidbrögd þess vid 100 MW rafmagns-framleidslu: ISOR, Iceland Geosurvey.
Hjartarson A., and Juliusson E., 2007, Reiknilíkan af jarðhitakerfinu á Reykjanesi og spár um viðbrögð þess við 100 MW rafmagns-5 framleiðslu: ISOR, Iceland Geosurvey, 2007/025, 145 p. (in Icelandic).

Holland, T. J. B., and Powell, R., 1998, An internally-consistent thermodynamic dataset for phases of petrological interest: Journal of Metamorphic Geology, v. 16, p. 309–344.
Hreggvidsdottir, H., ms, 1987, The greenschist to amphibolite facies transition in the Nesjavellir hydrothermal system, southwest Iceland: Stanford, California, Stanford University, Masters Thesis, 60 p.
Jakobsson, S. P., Jónsson, J., and Shido, F., 1978, Petrology of the Western Reykjanes Peninsula, Iceland: Journal of Petrology, v. 19, p. 669–705, doi:10.1093/petrology/19.4.669.
Johnson, J. W., and Norton, D., 1991, Critical phenomena in hydrothermal systems: State thermodynamic, electrostatic, and transport properties of H_2O in the critical region: American Journal of Science, v. 291, p. 541–648.
Johnson, J. W., Oelkers, E. H., and Helgeson, H. C., 1992, Supcrt92: A software package for calculating the standard molal thermodynamic properties of minerals, gases, aqueous species, and reactions from 1 bar to 5000 bar and 0 degrees Celsius to 1000 degrees Celsius: Computers and Geosciences, v. 18, p. 899–947, doi:10.1016/0098-3004(92)90029-Q.
Karingithi, C. W., Arnórsson, S., and Gronvold, K., 2006, Hydrothermal mineral buffers controlling reactive gas concentrations in the Olkaria geothermal system, Kenya: Unpublished, University of Iceland, 53 p.
Karlsdottir, R., 1998, A TEM-resistivity survey of Svartsengi high-temperature field in 1997: Orkustofnun report, OS-98025, 43 p. (in Icelandic).
Klein, C., 2002, The 22nd edition of the Manual of Mineral Science (after J. D. Dana): New York, John Wiley and Sons, Inc., 641 p.
Krauskopf, K. B., and Bird, D. K., 1995, Introduction to Geochemistry: San Francisco, McGraw Hill, 668 p.
Kristmannsdóttir, H., ms, 1970, Anorthositt og assosierte bergarter pa Hrappsey, Vest Island, Norway: Oslo, Norway, University of Oslo, Ph. D. Thesis, 162 p.
Larsen, G., Gudmundsson, M. T., and Bjornsson, H., 1998, Eight centuries of periodic volcanism at the center of the Iceland hotspot revealed by glacier tephrostratigraphy: Geology, v. 26, p. 943–946, doi:10.1130/0091-7613(1998)026<0943:ECOPVA>2.3.CO;2.
Liebscher, A., 2004, Spectroscopy of epidote minerals: Reviews in Mineralogy and Geochemistry, v. 56, p. 125–170, doi:10.2138/gsrmg.56.1.125.
Lonker, S. W., Franzson, H., and Kristmannsdóttir, H., 1993, Mineral-fluid interactions in the Reykjanes and Svartsengi geothermal systems, Iceland: American Journal of Science, v. 293, p. 605–670.
Marks, N., Schiffman, P., Zierenberg, R., Elders, W., and Fridleifsson, G., 2006, Iceland Deep Drilling Project: (VI) Fluid-rock Interactions in the Reykjanes Geothermal System as Indicated by Alteration Mineralogy and Sulfur Isotopes: San Francisco, California, American Geophysical Union, Fall Meeting 2006, Abstract #NG43A-1150.
Marks, N., Zierenberg, R., Schiffman, P., Elders, W., Fridleifsson, G., and Franzson, H., 2008, Alteration mineralogy, sulfur isotopes, and amphibole chemistry in the Reykjanes Geothermal System: Reykjavik, Iceland, International Association of Volcanology and Chemistry of the Earth's Interior General Assembly 2008.
Marty, B., and Tolstikhin, I. N., 1998, CO_2 fluxes from mid-ocean ridges, arcs and plumes: Chemical Geology. v. 145, p. 233–248, doi:10.1016/S0009-2541(97)00145-9.
Milodowski, A. E., Savage, D., Bath, A. H., Fortey, N. J., Nancarrow, P. H. A., and Shepherd, T. J., 1989, Hydrothermal mineralogy in geothermal assessment: Studies of Miravalles Field, Costa Rica and experimental simulations of hydrothermal alteration: British Geological Survey Technical Report WE/89/63, Fluid Processes Group Series, p. 81–82.
Mungania, J., 1993, Borehole geology of well RN-9, Reykjanes, SW-Iceland: United Nations Training Programme, Reykjavik, Iceland, Report 12, 38 p.
Naumov, G. B., Ryzheko, B. N., and Khodakovsky, I. L., 1971, Handbook of Thermodynamic Data: Moscow, Atomizdat, 239 p. (in Russian).
Norton, D. L., 1977, Fluid circulation in the Earth's crust, *in* Heacock, J. G., editor, The Earth's Crust: Its Nature and Physical Properties: American Geophysical Union, Monograph 20, p. 693–704.
——— 1979, Transport phenomena in hydrothermal systems: the redistribution of chemical components around cooling magmas: Bulletin of Mineralogy, v. 102, p. 471–486.
——— 1984, Theory of hydrothermal systems: Annual Review of Earth and Planetary Sciences, v. 12, p. 155–177, doi:10.1146/annurev.ea.12.050184.001103.
——— 1987, Advective metasomatism, *in* Helgeson, H. C., editor, NATO ASI Series, Series C: Mathematical and Physical Sciences, v. 218: Dordrecht-Boston, D. Reidel Publishing Company, p. 123–132.
——— 1988, Metasomatism and permeability: American Journal of Science, v. 288, p. 604–618.
——— 1990, Pore fluid pressure near magma chambers, *in* Bredehoeft, J. D., and Norton, D. L., editors, The Role of Fluids in Crustal Processes: Washington, D. C., National Academy Press, p. 42–49.
Norton, D. L., and Dutrow, B. L., 2001, Complex behavior of magma-hydrothermal processes: Role of supercritical fluid: Geochimica et Cosmochimica Acta, v. 65, p. 4,009–4,017, doi:10.1016/S0016-7037(01)00728-1.
Oelkers, E. H., Gislason, S. R., and Matter, J., 2008, Mineral carbonation of CO_2: Elements, v. 4, p. 333–337, doi:10.2113/gselements.4.5.333.
Ólafsson, J., and Riley, J. P., 1978, Geochemical studies on the thermal brine from Reykjanes (Iceland): Chemical Geology, v. 21, p. 219–237, doi:10.1016/0009-2541(78)90046-3.
Pálmason, G., Johnsen, G. V., Torfason, H., Saemundsson, K., Ragnars, K., Haraldsson, G. I., and Halldórsson, G. K., 1985, Evaluation of geothermal resources in Iceland: National Energy Authority Report OS-85076/JHD-10, 134 p. (in Icelandic).
Patrier, P., Beaufort, D., Meunier, A., Eymery, J. P., and Petit, S., 1991, Determination of the nonequilibrium ordering state in epidote from the ancient geothermal field of Saint Martin: Application of Mössbauer Spectroscopy: American Mineralogist, v. 76, p. 602–610.

Pope, E. C., Bird, D. K., Arnórsson, S., Fridriksson, Th., Elders, W. A., and Fridleifsson, G.Ó., 2009, Isotopic constraints on ice age fluids in active geothermal systems: Reykjanes, Iceland: Geochimica Cosmochimica Acta, v. 73, p. 4,468–4,488. doi:10.1016/j.gca.2009.03.033.

Ragnarsdóttir, K. V., Walther, J. V., and Arnórsson, S., 1984, Description and interpretation of the composition of fluid and alteration mineralogy in the geothermal system, at Svartsengi, Iceland: Geochimica et Cosmochimica Acta, v. 48, p. 1,535–1,553, doi:10.1016/0016-7037(84)90409-5.

Reed, M. H., 1982, Calculation of multicomponent chemical equilibria and reaction proceses in systems involving minerals, gases and an aqueous phase: Geochimica et Cosmochimica Acta, v. 46, p. 513–528, doi:10.1016/0016-7037(82)90155-7.

Reed, M., and Spycher, N., 1984, Calculations of pH and mineral equilibria in hydrothermal waters with application to geothermometry and studies of boiling and dilution: Geochimica et Cosmochimica Acta, v. 48, p. 1,479–1,492, doi:10.1016/0016-7037(84)90404-6.

Robie, R. A., and Hemingway, B. S., 1995, Thermodynamic properties of minerals and related substances at 298.15 K and 1 bar (10^5 Pascals) pressure and at higher temperatures: U.S. Geological Survey Bulletin, v. 2131, 461 p.

Saemundsson, K., 1997, Simplified geological and geothermal map of Reykjanes: Prepared by Okustofnun for Sudurnes Regional Heating, scale 1:10,000.

——— 2000, Cold climate and glacial vestiges in Iceland: in Iceland 2000: Modern Processes and Past Environments Conference Abstracts, p. 71–73.

Simmons, S. F., and Christenson, B. W., 1994, Origins of calcite in a boiling geothermal system: American Journal of Science, v. 294, p. 361–400.

Sleep, N. H., and Zahnle, K., 2001, Carbon dioxide cycling and implications for climate on ancient Earth: Journal of Geophysical Research, v. 106, n. E1, p. 1,373–1,399, doi:10.1029/2000JE001247.

Stefánsson, A., and Arnórsson, S., 2002, Gas pressures and redox reactions in geothermal fluids in Iceland: Chemical Geology, v. 190, p. 251–271, doi:10.1016/S0009-2541(02)00119-5.

Surdam, R. C., 1969, Electron microprobe study of prehnite and pumpellyite from the Karmutsen group, Vancouver Island, British Columbia: American Mineralogist, v. 54, p. 256–266.

Sveinbjörnsdóttir, Á. E., ms, 1983a, Hydrothermal metamorphism and rock water interactions in the Krafla and Reykjanes geothermal fields, Iceland: Norwich, England, University of East Anglia, Ph. D. thesis, 282 p.

——— 1983b, Water-rock interaction in Krafla and Reykjanes geothermal systems, Iceland: London, Journal of the Geological Society, v. 140, p. 549–550, doi:10.1144/gsjgs.140.4.0549.

——— 1992, Composition of geothermal minerals from saline and dilute fluids-Krafla and Reykjanes, Iceland: Lithos, v. 27, p. 301–315, doi:10.1016/0024-4937(91)90005-6.

Sveinbjörnsdóttir, Á. E., Coleman, M. L., and Yardley, B. W. D., 1986, Origin and history of hydrothermal fluids of the Reykjanes and Krafla geothermal fields, Iceland: A stable isotope study: Contributions to Mineralogy and Petrology, v. 94, p. 99–109, doi:10.1007/BF00371231.

Tómasson, J., and Kristmannsdóttir, H., 1972, High temperature alteration minerals and thermal brines, Reykjanes, Iceland: Contributions to Mineralogy and Petrology, v. 36, p. 123–134, doi:10.1007/BF00371183.

White, R. S., and Morton, A. C., 1995, The Iceland Plume and its influence on the evolution of the NE Atlantic: Journal of the Geological Society, London, v. 152, p. 935–1047, doi: 10.1144/GSL.JGS.1995.152.01.08

Wiese F., Fridriksson, Th., and Ármannsson, H., 2008, CO2 fixation by calcite in high-temperature geothermal system in Iceland: Iceland GeoSurvey Report\'d3 NEEDS\'cd NEEDS SOR-2008/003.